Politecnico di Torino
Department of Applied Science and Technology
NANOTECHNOLOGIES FOR ICTs

Carbon-dots supported ferrites for teragnostic applications: synthesis and characterization

Master thesis project of:
Andrea Orlando

Supervisors:
Prof. Alberto Tagliaferro
Dott. Mattia Bartoli

July 2021

Abstract

Novel theranostic tool based on nitrogen-doped carbon dots and ferrite nanoparticles is reported. carbon dots are sp^2 and sp^3 hybridized carbon-based particles with sizes in the range of 1-10 nm. The properties that can be used in the medical field are their biocompatibility, high functionalizability, solubility in water photoluminescence and ease of preparation. Ferrite nanoparticles of zinc, nickel, zinc-nickel and bismuth are also prepared. Their properties include cytotoxicity, magnetism, ease of preparation. A simple and effective protocol of conjugation between carbon dots and ferrites is proposed. Carbon dot-ferrite conjugates are good candidates for imaging and tumor treatment applications such as localized phototherapy, hyperthermia, chemotherapy and drug delivery. Carbon dots are prepared through sonication of the citric acid and p-phenylenediammine precursors. A set of samples with the surfactant polyethylene glycol is also prepared and characterized to study its effect on the final structure of the carbon dots. A database of carbon dots treated at different temperatures (250 °C, 350 °C, 450 °C, 550 °C) is created and characterized. Ferrite nanoparticles were prepared through solid-state reaction (zinc, nickel and zinc-nickel ferrites) and sol-gel method (bismuth ferrite). Full-charaterization of carbon dots, ferrite nanoparticles and conjugations is performed using Raman spectroscopy, Fourier-transform infrared spectroscopy, fluorimetry and scanning electron microscopy equipment, showing good reproducibility and reliability.

Graphical abstract

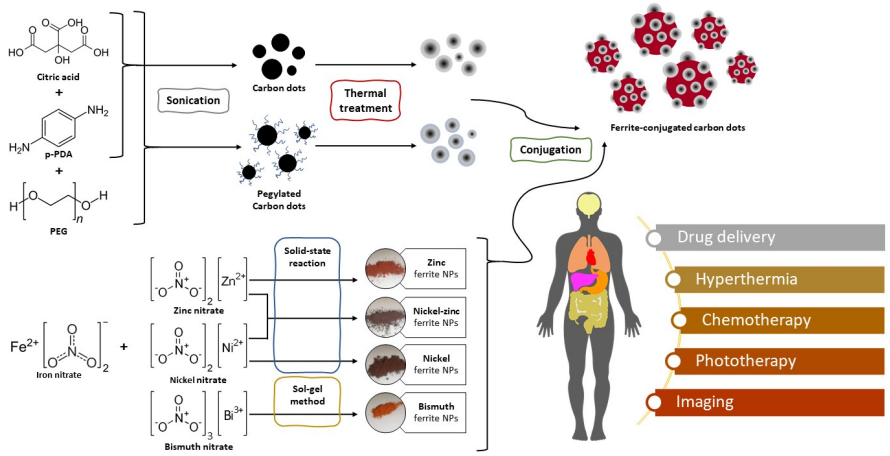

Contents

List of Figures

List of Tables

List of Acronyms

MRI	Magnetic resonance imaging
CD	Carbon dot
FNP	Ferrite nanoparticle
CA	Citric acid
p-DPA	p-Phenylenediammine
PEG	Polyethylene glycol
ZFO	Zinc ferrite
NFO	Nickel ferrite
ZNFO	Zinc-nickel ferrite
BFO	Bismuth ferrite
PL	Photoluminescence
FT-IR	Fourier-transform infrared spectroscopy
ATR	Attenuated total reflection
FESEM	Field-emission scanning electron microscope

To Nino, you are always with me.

Introduction 1

Nanotechnology is getting more and more diffused in basically all the technological and scientific fields. Energy[1], biomedical[2], electronic[3], material sciences[4] and a variety of fields are embracing the benefits that nanotechnology offers them in terms of improving efficiency, discovering new techniques and technologies, developing new frontiers of innovation. Nanomedicine is one among the most promising challenges in the medical field for this century[5]. This sciences-combining area comprehends drug[6] and RNA[7] delivery, detection of pathogens[8] or proteins[9], MRI contrast enhancement[10], vaccine development[11], antibacterial treatments[12], teragnostic tools[13], wearable devices[14], implants[15]

[1]Alktranee, "Applications of nanotechnology with hybrid Photovoltaic/Thermal systems".

[2]Nag, Sapra, and Mukhopadhyay, "Recent progress for nanotechnology-based flexible sensors for biomedical applications".

[3]Sangwan and Hersam, "Neuromorphic nanoelectronic materials".

[4]Z. Tang et al., "Phosphorus Science-Oriented Design and Synthesis of Multifunctional Nanomaterials for Biomedical Applications".

[5]Cheon, Chan, and Zuhorn, "The Future of Nanotechnology: Cross-disciplined Progress to Improve Health and Medicine".

[6]Deng et al., "Application of the Nano-Drug Delivery System in Treatment of Cardiovascular Diseases".

[7]Kim, Jozic, and Sahay, "Naturally Derived Membrane Lipids Impact Nanoparticle-Based Messenger RNA Delivery".

[8]Alafeef, Moitra, and Dipanjan Pan, "Nano-enabled sensing approaches for pathogenic bacterial detection".

[9]Nehra et al., "Nano-Biosensing Platforms for Detection of Cow's Milk Allergens: An Overview".

[10]H. Hu, "Recent Advances of Bioresponsive Nano-Sized Contrast Agents for Ultra-High-Field Magnetic Resonance Imaging".

[11]Shin et al., "COVID-19 vaccine development and a potential nanomaterial path forward".

[12]Dat et al., "Synthesis, characterization, and antibacterial activity investigation of silver nanoparticle-decorated graphene oxide".

[13]Zarei et al., "Theragnostic Magnetic Core-Shell Nanoparticle as Versatile Nanoplatform for Magnetic Resonance Imaging and Drug Delivery".

[14]Ko, Huang, and Lin, "Green technique solvent-free fabrication of silver nanoparticle–carbon nanotube flexible films for wearable sensors".

[15]X. Li et al., "Antimicrobial nanoparticle coatings for medical implants: Design challenges and prospects".

and many other research fields.

Since many structures of the cells of an organism are in the nanoscale, it is immediate to see that the ability to manipulate and condition processes at this scale becomes crucial in many cases. Nanoparticles promise to succeed in this challenge dues to their unique characteristics compared to their compound counterparts in the micro or macroscale. Nanocompounds can more easily cross many barriers present in the human body, even the most selective ones such as the blood-brain barrier (BBB). A further observation is related to the surface/volume ratio of these compounds with respect to the counterparts. Indeed, the smaller the size of a structure, the larger the role of the surface becomes relative to the volume. This helps to increase the efficiency of engineered and nanostructured materials by improving, for example, the selectivity of nanosensors having functionalized groups on the surface[16].

The first nanoformulated drug first appeared on the market in the middle 90s[17], and according to recent reviews , today there are more than 50 different commercially available nanomedicines and nanotechnology-based medical devices, with more than 400 in clinical trial phase[18]. The number of patents and applications is set to rise in the coming years, following the growing trend of this field.

Nowadays, 65% of experimental nanomedicines concerns the diagnosis and treatment of cancer. Nanomedicine can offer more effective therapies and faster and more accurate diagnostic methods than traditional approaches[19]. Furthermore, it can permanently eliminate the numerous side effects of today's anti-tumor therapies (for example, by delivering the drug locally). The predictable success of nanomedicine has been helped by the numbers: the anti-tumor nano-drugs being tested have a success rate of 94%[20]. Forecasts suggest that the success rate at the approval stage will be around 6%, while that of traditional anti-cancer therapies is 3.4%[21]. The factors that are holding back the rise of these technologies the most are numerous. Among them, the lack of clinical and safety protocols and the difficulty of scaling-up should be

[16]al., "Nanotechnology and Nanomedicine: Start small, think big".

[17]Choi and Han, "Nanomedicines: current status and future perspectives in aspect of drug delivery and pharmacokinetics".

[18]Germain et al., "Delivering the power of nanomedicine to patients today".

[19]T. Li et al., "Nanotechnology, an alternative with promising prospects and advantages for the treatment of cardiovascular diseases".

[20]He et al., "Survey of Clinical Translation of Cancer Nano medicines, Lessons Learned from Successes and Failures".

[21]Wong, Siah, and Lo, "Estimation of clinical trial success rates and related parameters".

mentioned[22,23].

There are, however, some limiting factors in the growth of this technology. Some challenges are delaying the definitive entry of nanotechnologies as an aid or replacement of traditional medicine. In particular, nanopharmaceuticals, as described by Wu et al.[24], have a large and intrinsic polydispersivity due to their complex chemical structure. This limits the actual throughput in the face of commercial demand because stability, manufacturing and efficiency controls are very demanding. In this framework, it is interesting to mention what happened with the first nanomedicine on the market (Doxil®, 1995). Due to sterility and manufacturing issues, its production was interrupted in November 2011. Until 2014 the shortages of the drug were sufficient, but subsequently the company had to develop an alternative manufacturing process, relentlessly raising the price of the treatment and delaying the therapies for patients. The manufacturing process is very important in the scale-up of this technology. In the laboratory phase, depending on whether the production method followed is of the "top-down" or "bottom-up" type (Figure 1.1[25]), often not optimized processes (sonication, centrifugation, milling, cross-linking, homogenization, etc.) are used for large-scale production in an industrial environment. There are also safety and toxicity challenges. Also due to their complex chemical structure, it is very important to absolutely check the quality of the final product. Indeed, even a small variation of the process conditions (quantities, ratios, reaction temperatures, process environment) can lead to the inefficiency of the product, or even make it dangerous for health. For this reason it is very important to study the toxicity of nanodrugs *in vivo* and in the long term. Unfortunately today the safety protocols for the tests of traditional medicines seem inadequate to carry out this type of checks. For this reason, more effective and advanced tools must be developed to ensure sustainable growth of this sector.

[22]Bremer-Hoffmann, Halamoda-Kenzaoui, and Borgos, "Identification of regulatory needs for nanomedicines".

[23]Wu, D. Wang, and Z. Li, "Grand challenges in nanomedicine".

[24]Ibid.

[25]Adapted from Sharma, A., Das, J. Small molecules derived carbon dots: synthesis and applications in sensing, catalysis, imaging, and biomedicine. J Nanobiotechnol 17, 92 (2019). https://doi.org/10.1186/s12951-019-0525-8

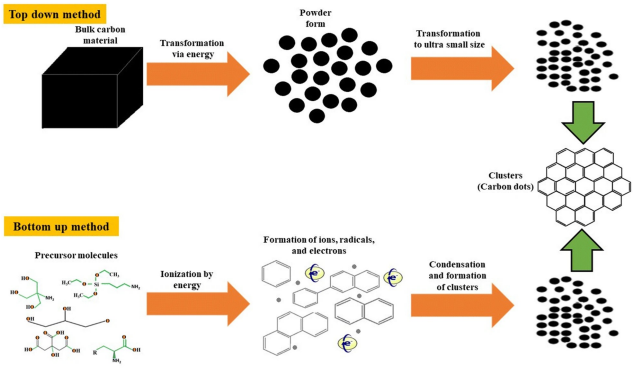

Figure 1.1: Bottom-up and top-down production approaches of carbon dots

In this thesis project I will present and analyze a combination of biomedicine, nanotechnology and materials science aiming to create a new teragnostic method for tumors based on the conjugation between carbon dots and ferrite nanoparticles. The idea is to effectively combine the properties of both precursors to obtain a biocompatible, functionalizable and effective method in numerous possible applications to fight tumors and other diseases.

Carbon Dots 2

CDs are among the novel nanoparticles appearing in the nanomedicine. They have been discovered in the early 21st century[26] but their use in human medicine is still subject of debate. The doubts arise from the fact that since CDs tend to be some very disordered arrangements, the internal structure is not well defined, as well as the electronic properties. Furthermore, these properties vary greatly depending on the method followed for the preparation of the CDs, so a bit of clarity is needed.

CDs can be referred as to zero-dimensional carbon nanoparticles since their lateral dimensions are in the nanometer range[27]. They can be divided into groups according to the method of preparation and therefore to their chemical, physical, electronic and structural characteristics, some of these groups are:

- **Black carbon dots (B-CDs)** are prepared through a top-down method (i.e., by starting from a carbon nanopowder and by reducing the dimensions of the particles via acidic oxidation). Their applications involve specific drug delivery to calcified bones[28] and along the BBB, through which they can cross[29].
- **Carbon nitride dots (CNDs)** preparation on the contrary follows a bottom-up method using an acid and an amine microwaved in order to perform condensation and then carbonized. Their applications are related to the ability of CNDs to target glioblastoma cells as well as the blood-brain barrier[30].
- **Yellow carbon dots (Y-CDs)** are prepared in a similar way to the CNDs but using a sonication process to mix and let the precursors

[26]Riggs et al., "Strong Luminescence of Solubilized Carbon Nanotubes".
[27]Mintz et al., "A deep investigation into the structure of carbon dots".
[28]Peng et al., "Carbon dots: promising biomaterials for bone-specific imaging and drug delivery".
[29]Mintz et al., "A deep investigation into the structure of carbon dots".
[30]Ibid.

react and perform condensation. They have a good penetrating ability, including the central nervous system[31].

- **Graphene quantum dots (GQDs)**, which are produced via both top-down[32] (such as nanotubes and graphene sheets cutting), and bottom-up methods (some precursors examples are citric acid[33] and glucose[34]). Their applications involve bioimaging[35], drug delivery[36], antibacterial and improving anticancer activity[37].
- Several different groups such as **polymer carbon dots**[38], **doped carbon dots**, etc.

In addition to the unique properties of each group, the whole family of CDs share some common interesting characteristics. They are biocompatible, water soluble, photoluminescent[39] and their synthesis is almost always low-cost. Indeed, studies have been carried out about the possibility to obtain high quality CDs from several types of waste materials (fruit and vegetable juices, plants, agro-industrial waste, human and domestic waste etc.)[40].
In this work the characteristics of the Y-CDs will be investigated, explaining their role in possible biological applications, the preparation procedure, the results of the analysis carried on the prepared samples.

2.1 Y-CDs preparation

Y-CDs are prepared following a bottom-up method using citric acid (CA) and para-phenylenediamine (p-PDA) as precursors. To study the production mech-

[31] Mintz et al., "A deep investigation into the structure of carbon dots".
[32] Dengyu Pan et al., "Hydrothermal Route for Cutting Graphene Sheets into Blue-Luminescent Graphene Quantum Dots".
[33] Dong et al., "Blue luminescent graphene quantum dots and graphene oxide prepared by tuning the carbonization degree of citric acid".
[34] L. Tang et al., "Deep Ultraviolet Photoluminescence of Water-Soluble Self-Passivated Graphene Quantum Dots".
[35] Zhu et al., "Strongly green-photoluminescent graphene quantum dots for bioimaging applications".
[36] Sheng et al., "pH-sensitive drug delivery based on chitosan wrapped graphene quantum dots with enhanced fluorescent stability".
[37] Zheng et al., "Glowing Graphene Quantum Dots and Carbon Dots: Properties, Syntheses, and Biological Applications".
[38] Xia et al., "Carbonized Polymer Dots with Tunable Room-Temperature Phosphorescence Lifetime and Wavelength".
[39] Zhao et al., "Spectroscopic studies of the optical properties of carbon dots: recent advances and future prospects".
[40] M. L. Liu et al., "Carbon dots: synthesis, formation mechanism, fluorescence origin and sensing applications".

anism with a surfactant in solution, a branch of CDs with 1:1 concentration of polyethylene glycol (PEG) with respect to CA was prepared and characterized (Figure 2.1).

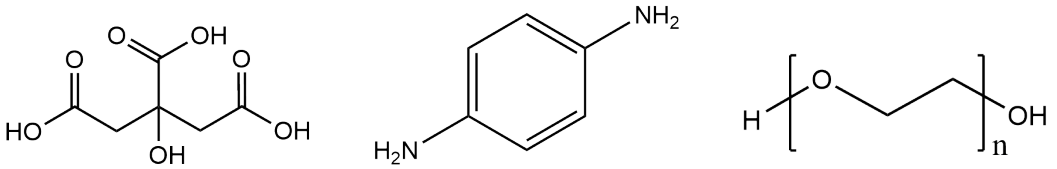

Figure 2.1: The precursors used to synthesize carbon dots: a) citric acid, b) p-phenylenediamine and c) polyethylene glycol

They are sonicated with a tip sonicator in an aqueous solution and then oven dried. The resulting powder is collected and cured in temperature. A set of different temperatures lead to the preparation and characterization of a set of different CDs. In particular, the CDs are treated at 250 °C, 350 °C, 450 °C and 550 °C in nitrogen. After the thermal process, they are purified by bringing them into an aqueous solution (with the help of a sonic bath to eliminate any agglomerates) and, subsequently, centrifuged. The liquid part is taken and dried in the oven. The resulting black powder is collected and analyzed. Further details of the preparation procedures are described in Section 4.

2.2 Y-CDs properties

Y-CD present lateral dimensions of 2-3 nm. They are carbon nanoparticles composed by a core of sp2 and sp3 hybridized carbon with N-groups coming from the p-PDA. The density and the number of N-groups is related to the preparation setup (annealing temperature and time).

Carbon dots have the important characteristic of being biocompatible. In fact, while the nanomedicine of the last few years has suffered a slowdown also due to the possible toxicity of the metals, oxides and rare earths used, biocompatibility of CDs has been proven by numerous studies. HeLa and Madin-Darby Canine Kidney cells have been shown to be fully compatible after 24 and 48 hours of incubation with CDs[41], with about 100% of viability. The excretion of CDs was tested by analyzing the urine of mice and measuring an increasingly lower concentration in the days following exposure, demonstrating that the renal apparatus of the animals effectively filtered the carbon

[41] Edison et al., "Microwave assisted green synthesis of fluorescent N-doped carbon dots: Cytotoxicity and bio-imaging applications".

dots administered intravenously[42]. In addition, organs to which doses of CDs were administered were examined and scanned. They showed no lesions or irregularities with respect to normal characteristics, indicating low toxicity and no inflammatory response from them[43]. furthermore, Y-CDs attracted a lot of attention since their discovery as they proved capable of bypassing the zebrafish's BBB, proving them to be excellent nanocarriers[44] for the central nervous system. In particular, the study by Leblanc et al. focused on the possible application of Y-CDs in brain diseases such as Alzheimer's Disease (AD)[45]. The ability of these CDs to bypass BBB is an important feature that distinguishes them from many drugs currently in use to fight against AD symptoms. Indeed, the role of the BBB is to behave as a barrier to prevent pathogens in the blood flux to reach the central nervous system. This is the reason why it is challenging to realize an efficient drug delivery protocol though the BBB.

One among the most useful characteristics of CDs is their photoluminescence. Several studies have been carried out to figure out the exact mechanism which creates this phenomenon. The complexity of the CDs structure still makes this difficult to achieve today. The basic idea is that the N-groups tend to passivate the surface of the dot, making the nanoparticle free of surface states. In this framework the PL effect is excitation independent. Clearly, on the surface several groups (carbonyl, carboxyl, amino-N) are present along with their specific trap states in the $\pi - \pi^*$ gap of the quasi-graphitic carbon core. These surface states have the ability to tune the emission of the CDs depending on their configuration, which in turn can be set during the synthesis procedure. In fact, the core of the CD acts as a HOMO-LUMO structure, with the HOMO and LUMO levels represented by the π and π^* energy levels, respectively. Trap levels within the gap can be related to oxygen and nitrogen doping which create specific intermediate states. Since the undoped HOMO-LUMO gap (HLG) is around 4 eV its characteristic emission is in the near-UV range[46] ($\lambda \approx 300$ nm). This value is conditioned by many factors, including the size of the CDs, their internal structure, and, as mentioned before, the type of doping. The presence of trap levels can red-shift the emission towards the VIS range or even the near-IR range. This characteristic is very important in biological imaging applications because (unlike the UV ones) long wavelength photons

[42] J. Liu et al., "One-Step Hydrothermal Synthesis of Nitrogen-Doped Conjugated Carbonized Polymer Dots with 31% Efficient Red Emission for In Vivo Imaging".

[43] Bao et al., "In vivo theranostics with near-infrared-emitting carbon dots—highly efficient photothermal therapy based on passive targeting after intravenous administration".

[44] Zhou et al., "Nontoxic amphiphilic carbon dots as promising drug nanocarriers across the blood–brain barrier and inhibitors of β-amyloid".

[45] Ibid.

[46] M. Liu, "Optical Properties of Carbon Dots: A Review".

can easily pass through biological tissues (skin, organs, fluids) providing an efficient imaging tool[47]. Several studies have been carried out in order to tune the emission properties of CDs depending on their doping and dimensions. Nitrogen doping is by far the most used and reported[48], but also fluorine , chlorine, selenium[49] and other elements are used.

The most promising feature of Y-CDs is related to the extraordinary functionalizability of their surface. In fact, on the external structure there are carbonyl groups, carboxyl groups, amino groups and hydroxyl groups deriving from the structure of the precursors. These functional groups can be engineered using them as a conjugation site with specific molecules or compounds (e.g. drugs, lipids, proteins and other biomolecules[50] or, as in this case, inorganic compounds such as ferrites).

[47]Ma et al., "Deep learning for in vivo near-infrared imaging".

[48]Jiang et al., "Photoactivated Fluorescence Enhancement in F,N-Doped Carbon Dots with Piezochromic Behavior".

[49]Y. Hu, Gao, and Luo, "Fluorescence detection of malachite green in fish tissue using red emissive Se,N,Cl-doped carbon dots".

[50]C. C. Wang et al., "Cu2+-induced quenching and recovery of the luminescence of dopamine-conjugated carbon dots for sensing deferasirox in plasma".

Ferrite nanoparticles 3

The applications of nanoparticles in the medical field are more and more. Metals, polymers, ceramics, oxides, lipids, proteins, variegated compounds have been studied, developed and applied for years to treat, diagnose and prevent many diseases. In this work the focus is on the production and characterization of various spinel ferrite nanoparticles (FNPs).
A spinel ferrite is a compound of the type AB_2O_4, in which A and B are metal cations and occupy respectively the tetrahedral and octahedral site of the spinel crystallographic structure. Spinel ferrite nanoparticles are used in many technological and medical fields as catalysts[51] and adsorbents (for example in wastewater treatments[52]), MRI contrast enhancers[53], tumor hyperthermia treating tools[54], drug delivery agents and antimicrobial agents[55]. Their main characteristics are paramagnetism, cytotoxicity and ease of synthesis.

FNPs are produced following several possible procedures, including bottom-up (sol-gel[56], co-precipitation[57], thermal decomposition[58]) and top-down methods[59].
In this work the synthesis and characterization of bismuth ($BiFeO_3$), zinc ($ZnFe_2O_4$), nickel ($NiFe_2O_4$) and nickel-zinc ($Ni_{0.5}Zn_{0.5}Fe_2O_4$) ferrites will

[51]Senapati, Borgohain, and Phukan, "Synthesis of highly stable CoFe2O4 nanoparticles and their use as magnetically separable catalyst for Knoevenagel reaction in aqueous medium".

[52]Qu, Alvarez, and Q. Li, "Applications of nanotechnology in water and wastewater treatment".

[53]Lee et al., "Recent Developments in Magnetic Diagnostic Systems".

[54]Reddy et al., "Magnetic Nanoparticles: Design and Characterization, Toxicity and Biocompatibility, Pharmaceutical and Biomedical Applications".

[55]Maksoud et al., "Synthesis and characterization of metals-substituted cobalt ferrite [Mx Co(1-x) Fe2O4; (M = Zn, Cu and Mn; x = 0 and 0.5)] nanoparticles as antimicrobial agents and sensors for Anagrelide determination in biological samples".

[56]Larumbe et al., "Sol-gel NiFe2O4 nanoparticles: Effect of the silica coating".

[57]Thakur, Rai, and Sharma, "Structural characterization and magnetic study of NiFexO4 synthesized by co-precipitation method".

[58]Zakiyah et al., "Up-scalable synthesis of size-controlled copper ferrite nanocrystals by thermal treatment method".

[59]Marinca, Chicinaş, and Isnard, "Structural and magnetic properties of the copper ferrite obtained by reactive milling and heat treatment".

be treated.

3.1 Ferrites preparation

The ferrites were prepared following two different approaches. The nickel, zinc and nickel-zinc ferrites were prepared following a solid state reaction of their nitrates at high temperatures in air. Bismuth ferrite was prepared following a sol-gel method with ethylene glycol as solvent. Several calcination temperatures and times have been tested, in this paper the procedures that have allowed to obtain the best results are reported. Further details of the preparation procedures are described in Section 4.

3.2 Ferrites properties

Since the intravenous route is the most used for the administration of nanoparticles for teragnostic purposes, it is important to consider the selectivity of the toxicity of NPs. In particular, they must not damage blood cells such as erythrocytes, leukocytes, etc., especially in drug delivery and cancer treatment applications (via hyperthermia of cytotoxicity).
A recent study[60] investigated the *in vitro* viability of erythrocytes and leukocytes in solution with NFO, ZFO and ZNFO up to 200 $\mu g/mL$ concentrations. No significant changes in cell viability were observed after treatment. On the other hand, ZNFO showed good cytotoxicity against human colon cancer (HT29), breast cancer (MCF7), and liver cancer (HepG2) cells, arresting proliferation and inducing apoptosis[61].
NFO nanoparticles have been proven to exhibit dose-dependent cytotoxicity. Viability was 69% in the sample exposed to an NFO concentration of 100 mg/L[62].
ZFOs have proved to be good candidates for cancer hyperthermia treatments due to their magnetic properties. Researchers[63] reported that a concentration of 2 mg/mL of ZFO nanoparticles can reach a temperature of 42 $°C$ with a magnetic field of 4 kA/m. However, the most promising feature of NFO is its cytotoxicity, linked to the presence of nickel in the crystalline sites of the ferrite

[60] Martínez-Rodríguez, Tavárez, and Sánchez, "In vitro toxicity assessment of zinc and nickel ferrite nanoparticles in human erythrocytes and peripheral blood mononuclear cell".
[61] Al-Qubaisi et al., "Cytotoxicity of nickel zinc ferrite nanoparticles on cancer cells of epithelial origin".
[62] Ahamed et al., "Oxidative stress mediated apoptosis induced by nickel ferrite nanoparticles in cultured A549 cells".
[63] Patade et al., "Preparation and characterisations of magnetic nanofluid of zinc ferrite for hyperthermia".

itself[64]. On the other hand, BFO nanoparticles have been proved fully biocompatible and good candidate for imaging applications. In fact, they have shown excellent cellular permeability and low cytotoxicity[65]. Another research[66] investigated the use of BFO nanoparticles as a dose-enhancer in radiotherapy, MRI contrast enhancer and magnetic hyperthermia mediator. The biocompatibility was tested greater than 95% for different concentrations of BF nanoparticles (0.05 to 1 mg/mL), while a solution of 7 mg/mL increased its temperature up to 50 $°C$ with a magnetic field intensity of 17.2 kA/m, a promising result for hyperthermia applications. Furthermore, the presence of bismuth makes the ferrite radiopaque and possibly usable in the radio-diagnostic field[67].

[64]Egizbek et al., "Stability and cytotoxicity study of NiFe2O4 nanocomposites synthesized by co-precipitation and subsequent thermal annealing".

[65]Staedler et al., "Cellular uptake and biocompatibility of bismuth ferrite harmonic advanced nanoparticles".

[66]Rajaee et al., "Multifunctional Bismuth Ferrite Nanoparticles as Magnetic Localized Dose Enhancement in Radiotherapy and Imaging".

[67]Shahbazi et al., "The versatile biomedical applications of bismuth-based nanoparticles and composites: therapeutic, diagnostic, biosensing, and regenerative properties".

Materials and Methods 4

4.1 Materials

Citric acid was purchased from Nortem Biotechnology. p-Phenylenediamine was purchased from Fluka. Polyethylene glycol 4000 was purchased from PHU Alpaca. Iron (III) nitrate nonahydrate was purchased from Carlo Erba Reagents. Zinc nitrate hexahydrate was purchased from Titolchimica. Nickel nitrate hexahydrate was purchased from Alfa Aesar. Bismuth nitrate pentahydrate was purchased from Fluka.
All chemicals used were of analytical grade and were used as received without any further purification.

The instruments used for the synthesis include a Vibra Cell sonicator (purchased from Sonics), a hot plate with magnetic stirring, a microcentrifuge MPW-55, a muffle furnace and a tubular Pyrex®reactor.

4.2 Synthesis of carbon dots

YCDs were prepared following the procedure reported by Leblanc et al. in their work[68]. 0.56 g of p-PDA and 0.04 g of CA were mixed in 10 mL of DI water and then sonicated at 42 kHz for 1 hour. The resulting purple solution was put to dry in an oven at 80 °C for 48 hours. The precipitate was pounded in a mortar to be prepared for heat treatment. The next step consisted in treating the CDs samples under argon gas in the muffle oven. Different temperatures made it possible to identify different sets of CDs. Four temperature values were used: 250 °C, 350 °C, 450 °C and 550 °C. The thermal process lasted for 10 minutes for all samples. Once extracted from the oven, the CDs were cooled to room temperature and subsequently dissolved in DI water for 10 minutes in a sonic bath to help dissolve and break up any aggregations. The obtained solution was then centrifuged at 10000 rpm for 10 minutes. After centrifugation, the residue was removed, and the liquid part dried at 80 °C for

[68]Mintz et al., "A deep investigation into the structure of carbon dots".

48h. In this way, only the CDs that were solubilized in water were obtained. Another set of CDs was prepared using PEG as a non-ionic surfactant. In this case, a quantity of PEG was added to the p-PDA and CA in a ratio of 1:1 with respect to CA. The heat treatment was done at 250 °C, and the centrifugation and extraction processes were the same as those of the other CDs.
Table 4.1 table summarizes the database of prepared CDs:

Name	**Annealing Temp.**	**Surfactant**
CD	-	-
CDPEG	-	PEG (1:1 with CA)
CDPEG-250	250 °C	PEG (1:1 with CA)
CD-250	250 °C	-
CD-350	350 °C	-
CD-450	450 °C	-
CD-550	550 °C	-

Table 4.1: Database of prepared carbon dots

4.3 Synthesis of ferrites nanoparticles

4.3.1 Synthesis of zinc ferrite nanoparticles

For the preparation of the ZFO nanoparticles a solid-state reaction approach has been followed. Iron (III) nitrate nonahydrate ($Fe(NO_3)_3 \cdot 9H_2O$, Fe 13.51% wt) and zinc nitrate hexahydrate ($Zn(NO_3)_3 \cdot 6H_2O$, Zn 21.85% wt) quantities were taken to obtain a Fe:Zn molar ratio of 2:1. The salts were crushed in the mortar and subsequently treated at 550 °C for 1 hour under nitrogen gas in the muffle furnace.

4.3.2 Synthesis of nickel ferrite nanoparticles

The preparation of the NFO nanoparticles followed a similar procedure. Iron (III) nitrate nonahydrate ($Fe(NO_3)_3 \cdot 9H_2O$, Fe 13.51% wt) and nickel nitrate hexahydrate ($Ni(NO_3)_2 \cdot 6H_2O$, Ni 20.18% wt) quantities were taken to obtain a Fe:Ni molar ratio of 2:1. After being pounded in the mortar they were treated at 550 °C in nitrogen gas for 1 hour.

4.3.3 Synthesis of zinc-nickel ferrite nanoparticles

For ZNFO nanoparticles, a mole fraction of Fe:Zn:Ni equal to 2:1:1 was considered. Again, the salts were pounded in a mortar and then treated at 550 °C for 1 hour under nitrogen gas.

4.3.4 Synthesis of bismuth ferrite nanoparticles

The preparation of the BFO nanoparticles involved a sol-gel method. 5 mmol of Iron (III) nitrate nonahydrate ($Fe(NO_3)_3 \cdot 9H_2O$) and 5 mmol of bismuth nitrate pentahydrate ($Bi(NO_3)_3 \cdot 5H_2O$) were dissolved in 12 ml of ethylene glycol. To facilitate the dissolution, the compound was stirred at 80 °C for about 30 minutes. The obtained solution, brown in color, was placed in the muffle furnace under nitrogen gas preheated to 400 °C and with a temperature ramp of 5 °C/min. Once reached 650 °C the temperature was stabilized, and the compound calcined for 30 minutes. The resulting gray powder was then further calcined in air at 550 °C for 1h to remove any remaining solvent.
Table 4.2 summarizes the database of prepared FNPs:

Name	**Synthesis**	**Annealing Temp.**
ZFO	Solid-state	550 °C
NFO	Solid-state	550 °C
ZNFO	Solid-state	550 °C
BFO	Sol-gel	From 400 °C to 650 °C with 5 °C/min, then 30 minutes at 650°C

Table 4.2: Database of prepared ferrite nanoparticles

4.4 Synthesis of ferrite-carbon dots conjugates

Several attempts have been made to conjugate ferrites and carbon dots to find the best method that would allow to obtain a good interaction between the particles. A first attempt with untreated CDs and some ferrites was made to analyze the results. In this framework, 100 mg of carbon dots and 100 mg of ferrite were put in solution with 50 mL of water. After 24 hours of mixing, the solution was dried for 24 hours in an oven at 80 ° C, without performing a centrifugation. The Raman analysis however showed a high carbon content in the sample, which also had a very low magneticity compared to the ferrites used as precursors. This fact suggested to carry out a purification through centrifugation to eliminate the water-solubilized CDs before proceeding with

the drying.
The second conjugation attempt was made with CD-250 and the same ferrites used in the first test. After 48 hours of mixing, the solution was immediately centrifuged. The supernatant had a color equal to the solutions of CDs, while a black residue was present. This suggested that the unconjugated CDs were in solution, while the FNPs conjugated CDs were on the deposit. To be sure of this, both the solution and the deposit were analyzed with IR spectroscopy. The results confirmed the initial assumptions: the dried supernatant was composed of CDs, while the deposit showed peaks relative to both the FNPs and CDs.
Finally, the definitive conjugation was performed using the second conjugation protocol. The precursors were the CD-350 as carbon dots, together with the four ferrites that were the best in Raman analyzes: ZFO, NFO, ZNFO and BFO.
Table 4.3 summarizes the pepared and analyzed ferrite-conjugated CDs.

Name	**Carbon dots**	**Ferrite nanoparticles**
Zn-CD	CD-350	ZFO
Ni-CD	CD-350	NFO
ZnNi-CD	CD-350	ZNFO
Bi-CD	CD-350	BFO

Table 4.3: Database of prepared ferrite-conjugated carbon dots

Results 5

5.1 Instrumentation

Raman analysis was performed with the Renishaw inVia™ InSpect confocal microscope. The wavelength of the laser was varied from green (514 nm) for the analysis of CDs to red (785 nm) for the analysis of FNPs and conjugations.

FT-IR (ATR mode) analysis was performed using Nicolet 5700 FT-IR Spectrometer from Thermo Fisher Scientific.

Photoluminescence spectra were collected with the PerkinElmer LS-55 fluorescence spectrometer.

A ZEISS Supra 40 Field Emission Scanning Electron Microscopy has been used to perform FESEM analysis.

5.2 Carbon dots

A first glimpse of the PL of the CDs can be seen using a UV lamp as a source of excitation. Figure 5.1 shows the PL of aqueous solutions (120 mg/L) of prepared carbon dots under a UV lamp (364 nm).

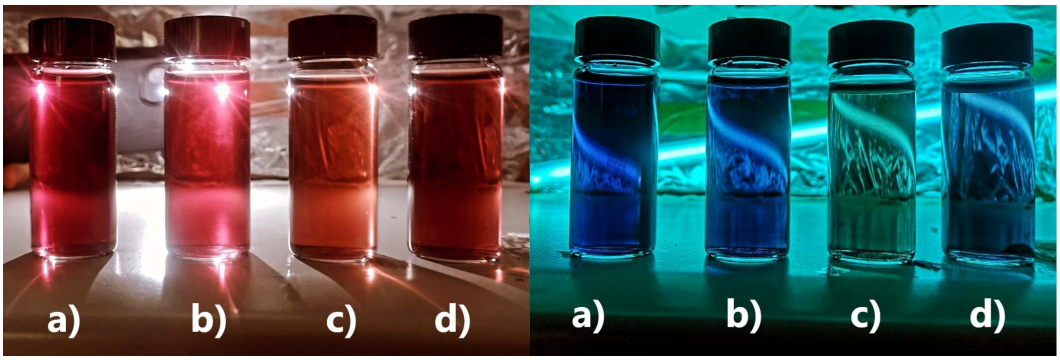

Figure 5.1: Carbon dots fluorescence under visible (left) and UV (right) light. Particles have been treated at different temperatures: a) 250 °C, b) 250 °C (PEG 1: 1), c) 350 °C and d) 450 °C

In Figure 5.2 the growth process of the CDs is schematically represented. As it can be seen, the reaction takes place mainly through the amidation between the carboxylic groups of the CA with the amino groups of the aromatic amine (p-PDA). The hydroxyl groups of CA can be part of the reaction, but due to the steric hindrance represented by the rest of the molecule, their contribution can be neglected. On the other hand, they help to obtain a structure rich in unsaturated carbons, and therefore rich in π bonds, useful for conjugation with ferrites. In fact, as seen in reaction 1) + 2), the hydroxyl group resulting from the AC helps to create a cyclic structure containing an N atom by means of an alcoholic elimination reaction. This process is more favored as the temperature rises. By increasing the temperature, in fact, dehydration and decarboxylation processes are promoted, increasing the degree of general aromatization and creating increasingly semi-graphitic structures. In this case, the advantage of using an aromatic amine as a precursor can be noticed. The NH_2 groups present on the p-PDA in fact have two growth points (nitrogen can make three bonds), so they help to obtain a much more condensed and ordered final structure. As seen in steps 1) and 2) in the figure, an amino group of the p-PDA can react with two molecules of CA, or with an NH_2 group of another amine.

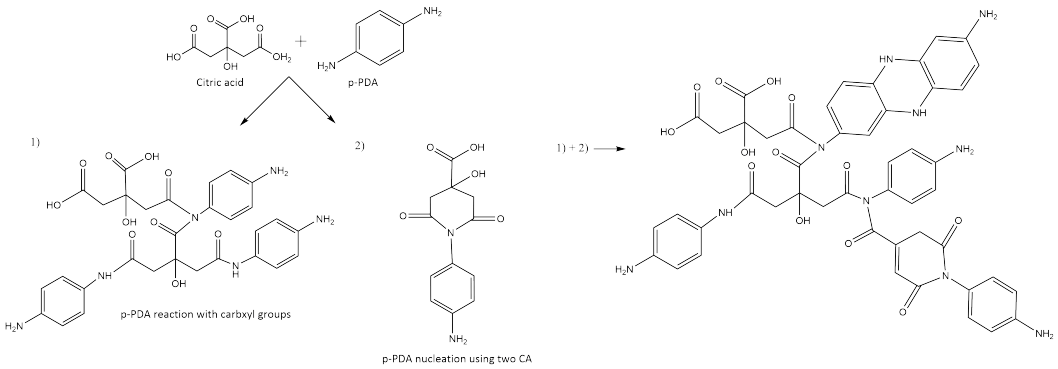

Figure 5.2: Nucleation process during the carbon dots formation starting from the precursors

5.2.1 FT-IR

CDs IR spectra are very useful to understand the structural and chemical conformation of samples. Through infrared spectroscopy, many absorption bands related to the bonds found in prepared nanoparticles can be uniquely identified. By comparing the spectra of precursors (AC and p-PDA) and CDs one can study the mechanism of growth supporting the reaction of the precursors themselves. Figure 5.3 shows the IR spectra of the two precursors and of the CDs obtained after sonication, not yet treated at temperature. As it can be seen, in the spectrum of the CA there are two peaks, one at 3500 cm^{-1} and a wider band between 3000 and 3500 cm^{-1}, related to the ν of the

OH bonds. The one with the highest energy is due to the ν of the OH of the hydroxyls, while the one on the left represents the band of carboxylic OH. The peak at 3500 cm^{-1} has a shoulder as the hydroxyl OH can interact with the carboxyl OH but also with another hydroxyl OH. The lower amplitude indicates that the latter case has a lower probability. On the other hand, it can be seen that the broadened band of carboxyls arises from the superposition of three peaks. In fact, if the three carboxylic groups present in the CA are labeled, it can be seen that we have two groups at the ends of the molecule (head) and one in the center of the same (center). They can therefore react to each other in three ways: head-head, head-center and center-center. Hence the birth of the three peaks. At 2750-2950 cm^{-1} one can see the peak related to the ν of saturated carbon. It is very low intensity as the CH bond has low dipole moment. The two peaks at 1800 cm^{-1} are related to the stretch of the C=O bond. The intensity confirms the high polarity of the bond. There are two peaks because the carboxyls can interact with themselves or with the non-carboxyl OH groups.

Switching to p-PDA, one can immediately notice the peaks of the NH ν between 3200 and 3400 cm^{-1}. At about 3000 cm^{-1} one can find the peak relative to the ν of the unsaturated CH of the aromatic ring. At 1700 cm^{-1} the peak relative to the δ of the C-N-H bond can be noticed, while the highest peak, at 1500 cm^{-1}, is due to the ν of the C=C (ring breathing). The last peak highlighted, at 1250 cm^{-1}, represents the ν of the CN bonds.

In the spectrum of CDs, the first thing one can notice is that the peak relating to the OH groups has disappeared, a sign that the CA groups have reacted, while the peak relating to the ν of the unsaturated CH of the aromatic rings remains. Another confirmation derives from the shifting of the peak of the C=O bond: now the carbon is also bonded to an N atom, weakening the bond and shifting its peak to the left.

As it can be seen in Figure 5.4, a study was also carried out through FT-IR to analyze the evolution of the internal and surface structure of CDs treated at different temperatures, as well as the effect of PEG. An important observation derives from the highest energetic peak of the NH bond stretches at 3400 cm^{-1}. By increasing the annealing temperature, the ratio between this peak (related to the presence of the primary amines) and those of the secondary and tertiary amines decreases more and more, until the peak of primary amines disappears when the samples are treated at 550 °C. This shows that temperature actually helps the amidation process by creating more and more condensed and ordered structures. The redistribution of the internal structure is also supported by the fact that the peaks at 3000 cm^{-1} are more broadened and less distinct from each other. Furthermore, we see how the skeletal modes are drastically cut off at 550 °C. It is probably a very graphitic and rigid structure, in which the functional groups have lost importance compared to the core structure. This is also demonstrated by the intensity decrement of the peak relative to the CN

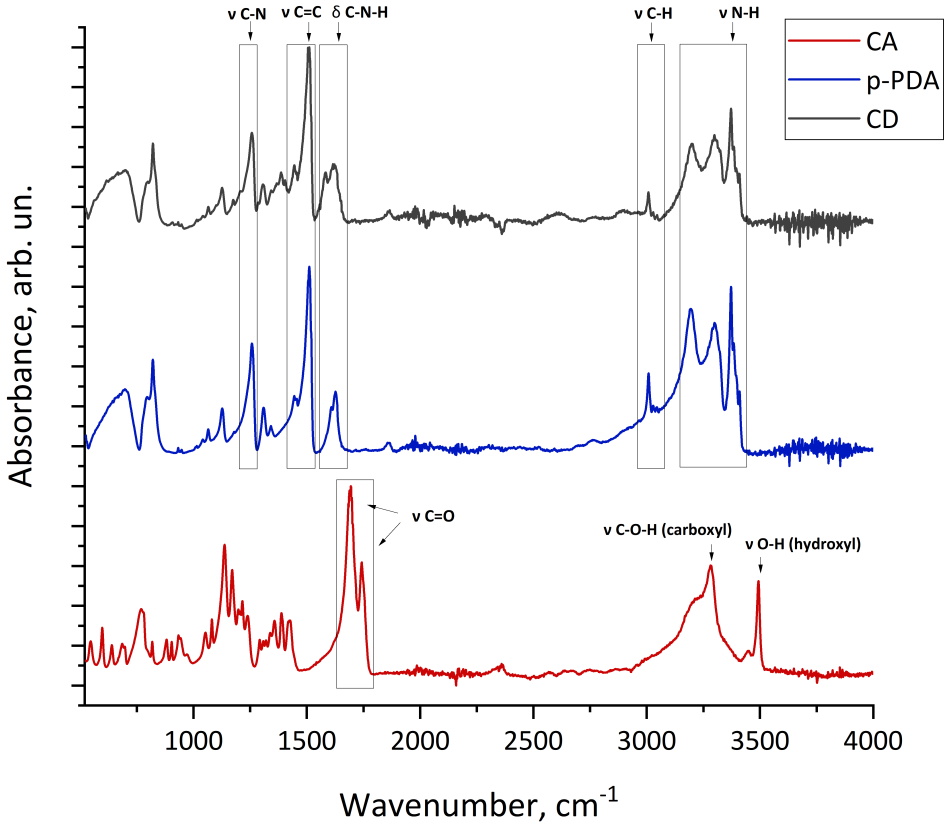

Figure 5.3: FT-IR spectra of the precursors and the obtained carbon dots

ν as the temperature rises, and by the increasing ratio of the ring breathing peak to the others.

5.2.2 Raman

The interpretation of the raman spectra of the CDs is not easy because the high fluorescence of the samples largely covers the signals deriving from the various functional groups and from the core of the nanoparticles. An attempt was made to identify peaks D and G (Figure 5.5), but their low intensity made it difficult to confirm their position with certainty. This indicates that aromatic structures have formed, but the resulting domains are not very large so they are localized structures. Overall, the structure of the CDs is very disordered and heterogeneous. Probably the bands of the CN and CH ν can be seen between the supposed peaks D and G, around 1500 cm^{-1}.

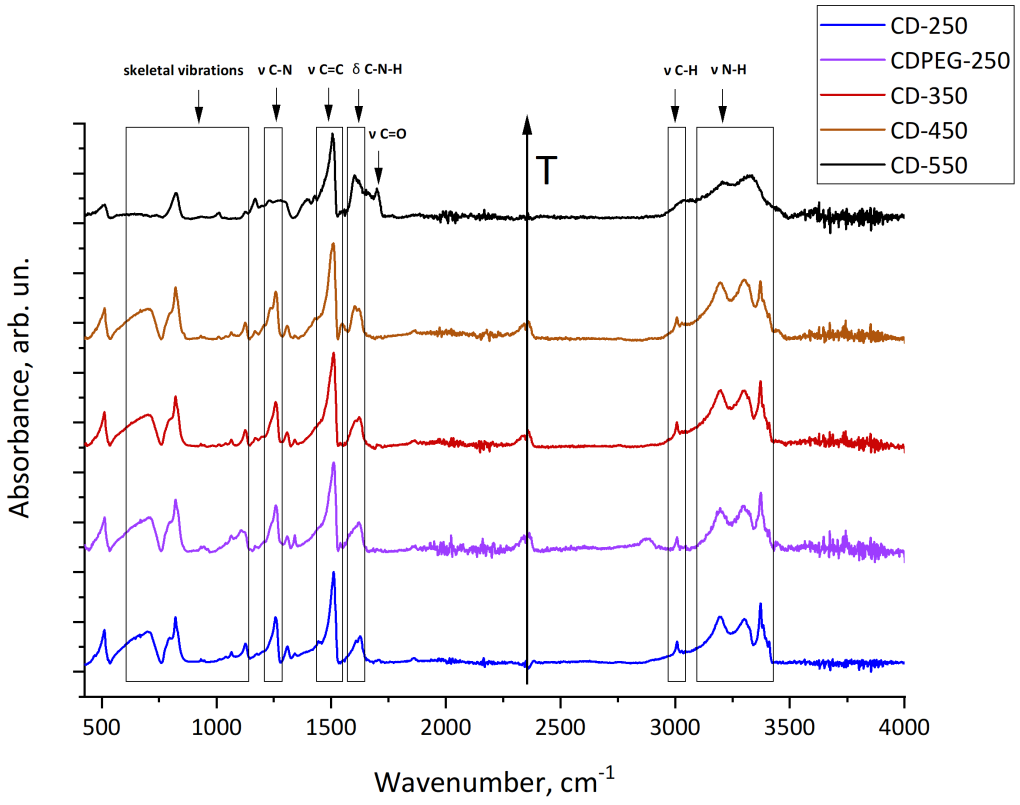

Figure 5.4: FT-IR spectra of carbon dots treated at different temperatures

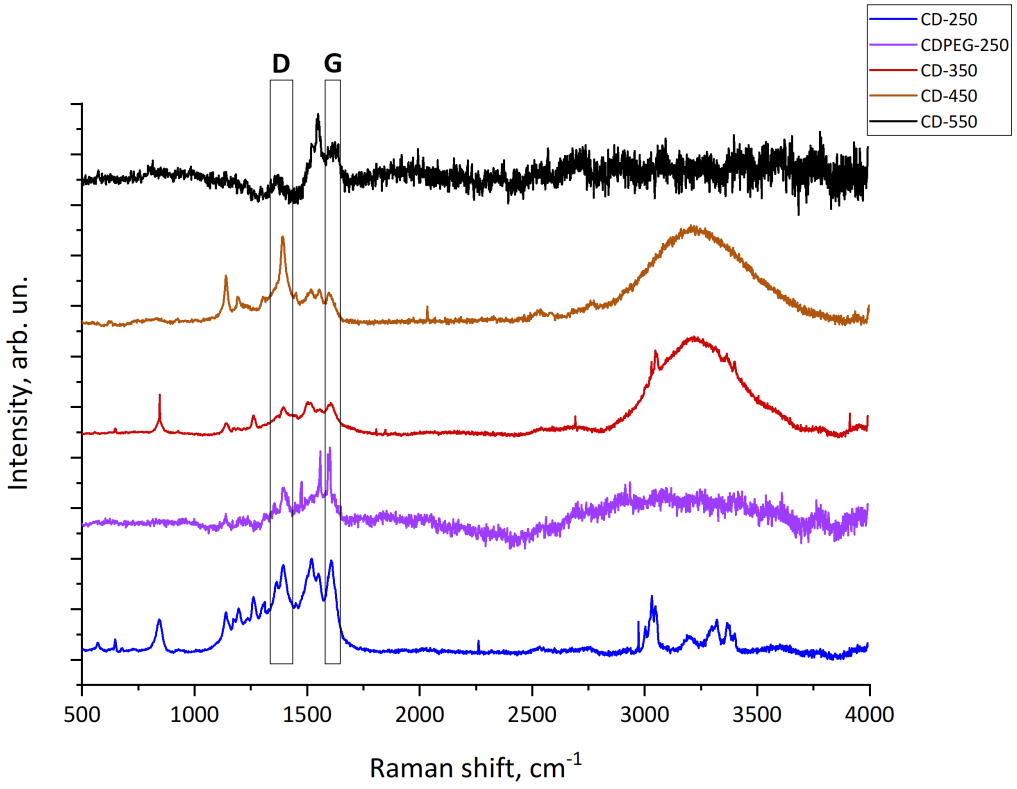

Figure 5.5: Raman spectra of carbon dots treated at different temperatures

From these spectra, however, one can try to understand what happens when the CDs are treated in temperature. In fact, looking at the bands present from 2900 cm^{-1} onwards, one can see the formation of a single band with CDs treated from 350 °C up. An exception is represented by the CDPEG-250 sample, where the single band is already noticeable at 250 °C. This indicates that a reorganization has taken place due to temperature, including dehydration and condensation. PEG helps to make this reorganization happen as it reduces the average size of the nanoparticles and induces their redistribution. It can be noticed that in the sample treated at 550 ° C the spectrum is reduced to a few bands: all the peaks related to the functional groups disappear. In this case a compound was obtained almost all graphitic, with still little large-scale organization as few functional groups such as carboxyl groups. This intake is confirmed by the fact that this sample is the only non-soluble in water: the functional groups have a lot of relevance with regard to water solubility.

5.2.3 Fluorometer

The optical properties of carbon dots have been mentioned and discussed above. For a complete characterization of the obtained CDs, fluorimeter analyzes were carried out to study the emission spectra of the nanoparticles with different excitation energies, from 275 nm (4.5 eV) to 525 nm (2.36 eV). The results are reported in Figures 5.6, 5.7, 5.8 and 5.9, which show the emission spectra of CD-250, CDPEG-250, CD-350 and CD-450, respectively. As it can be seen, two different types of emissions have been observed: an excitation-dependent emission (the prevailing one) and an excitation-independent one. Each set of CDs exhibited equivalent behavior, carrying both types of emission. This suggests the hypothesis that the emission of CDs is linked to the structure of the core of the nanoparticles. This is because the modification of functional groups on the surface when they are treated in temperature (as seen for example in the analysis of FT-IR results) does not affect evidently on the PL spectra of the CDs.

To study the trend of emission energy as a function of excitation energy, the graph in Figure 5.11 has been produced. As it can be seen, three excitation-independent emission bands were found, respectively at 1.7-1.9 eV, 2 eV and 3.2 eV. These emission bands represent radiative transitions within the core of the CDs. They could be attributed to the $\pi - \pi^*$ transition in the graphitic core of the nanoparticles, as well as to the orbitals resulting from the nucleation of the p-PDA. However, given that the internal structure of CDs is very complicated, it is difficult to uniquely attribute the source of this emission.

One would dare to say that the most interesting band of emission independent of the excitation is that at about 2 eV. This emission energy corresponds to a radiation of 635 nm. Therefore, the CDs act as down-converters of the exciting radiation ranging from near-UV up to 525 nm, emitting at a single wavelength in the visible range (bright red color). Both the ability to absorb

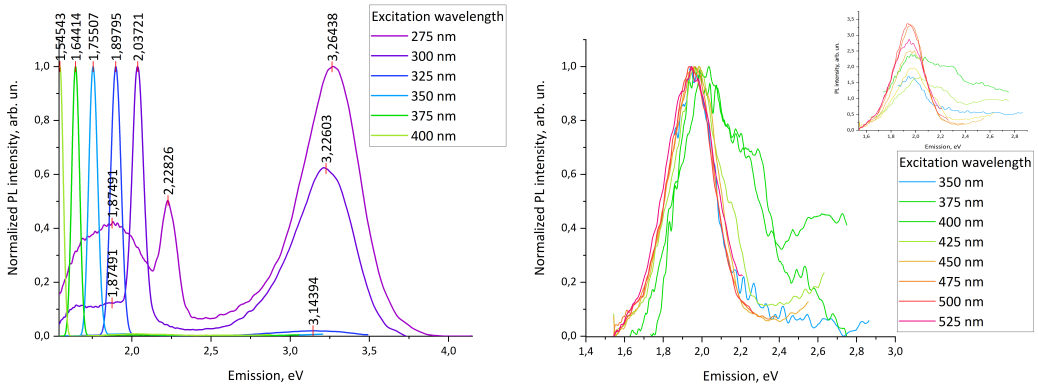

(a) (b)

Figure 5.6: Photoluminescence spectra of carbon dots treated at 250 °C: a) excitation-dependent emission and b) excitation-independent emission

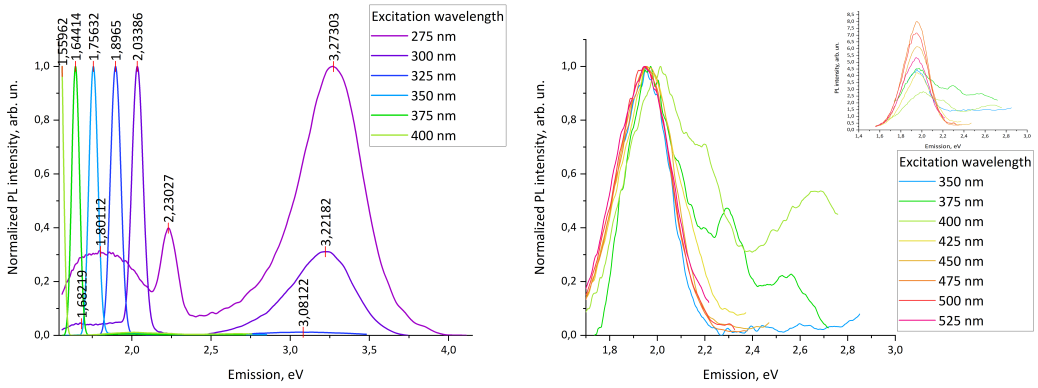

(a) (b)

Figure 5.7: Photoluminescence spectra of carbon dots treated at 250 °C with 1:1 ratio of PEG:AC: a) excitation-dependent emission and b) excitation-independent emission

UV and the quasi single-wavelength emission are very important characteristics in the medical field. The photons absorbed by the CDs can give rise to the photo-Fenton effect with the iron III of the ferrites, therefore a good absorption capacity is crucial. Furthermore, the red / orange radiation is one of the least absorbed by the tissues of the human body, making it very important in the field of diagnostic imaging (Figure 5.10[69]).

The excitation-dependent emission shows an almost perfectly linear behavior ($R^2 = 0.999$). The emission graph is common to all sets of CDs and can be

[69]Reprinted from Macmillan Publishers Ltd: Nature Nanotechnol., 2009, 4, 710–711. Copyright (2009).

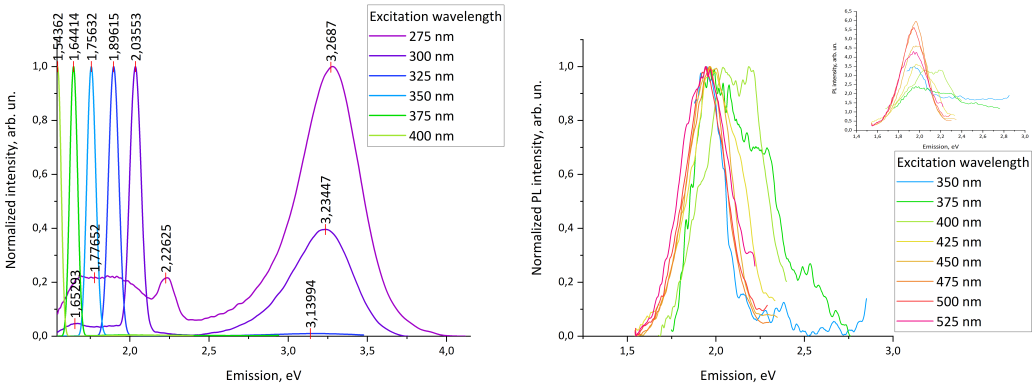

(a) (b)

Figure 5.8: Photoluminescence spectra of carbon dots treated at 350 °C: a) excitation-dependent emission and b) excitation-independent emission

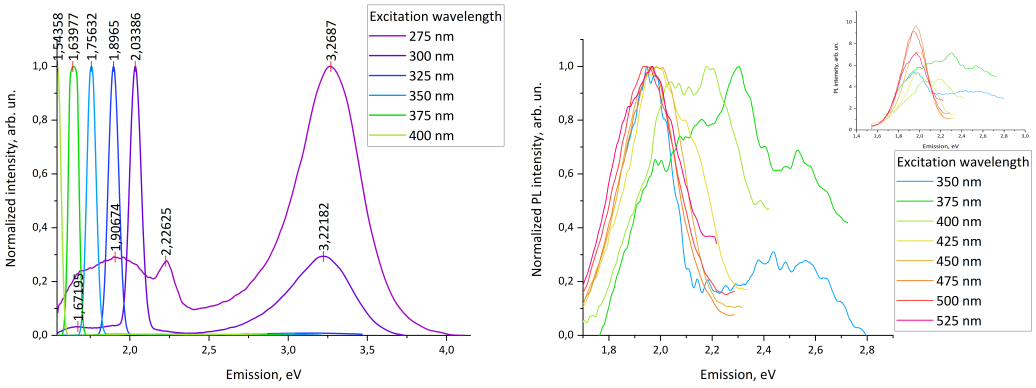

(a) (b)

Figure 5.9: Photoluminescence spectra of carbon dots treated at 450 °C: a) excitation-dependent emission and b) excitation-independent emission

modeled with a line with slope $K_0 = 0.47$.

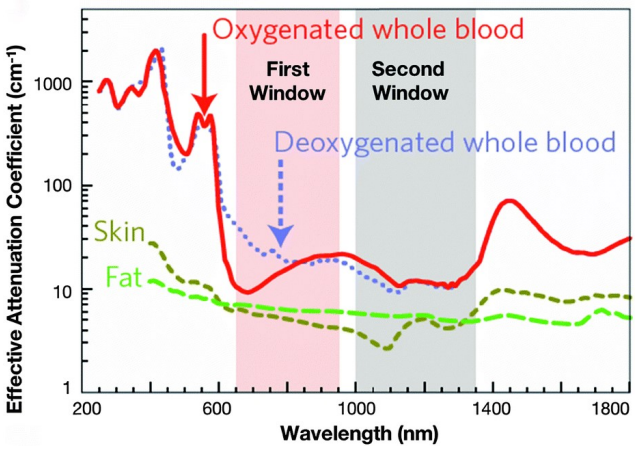

Figure 5.10: Absorption spectrum of some biological tissues and fluids

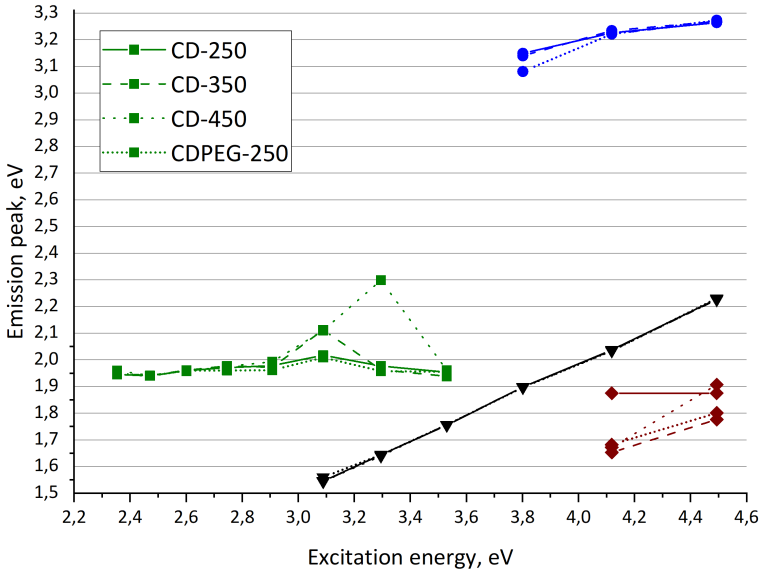

Figure 5.11: Emission bands as a function of excitation energy in carbon dots

5.3 Ferrite nanoparticles

The analysis of the FNPs was performed with a FESEM to check the morphology and size of the nanoparticles. Subsequently, Raman and FT-IR analyzes made it possible to characterize them at a compositional and structural level.

Figure 5.12 shows as an example an aqueous dispersion of the prepared nickel-zinc ferrites before and after applying a magnet to show their strong magnetism. A cuvette containing water is shown for reference.

(a) (b)

Figure 5.12: Aqueous dispersion of nickel-zinc ferrites a) before and b) after the application of a magnet. A cuvette containing water is shown for reference

5.3.1 FESEM

Images produced with FESEM showed excellent results obtained for all four prepared ferrite samples.

Looking at the ZFO (Figure 5.13), produced with solid-state reaction, we see a good homogeneity and oval-shaped, almost spherical nanoparticles.
The NFO (Figure 5.14) have a different morphology as they are very porous and there is evident layer by layer growth, even if the production method is identical to that of the ZFO NPs.
ZNFO can be said to show the signs of both of the above. The surface of the FNPs is very irregular and nanostructured (Figure 5.15), even if the irregularities are present in a fairly constant and homogeneous way on the nanoparticles.
Finally, looking at the BFO (Figure 5.16), produced with the sol-gel method, no particular morphological or size homogeneity is noted.

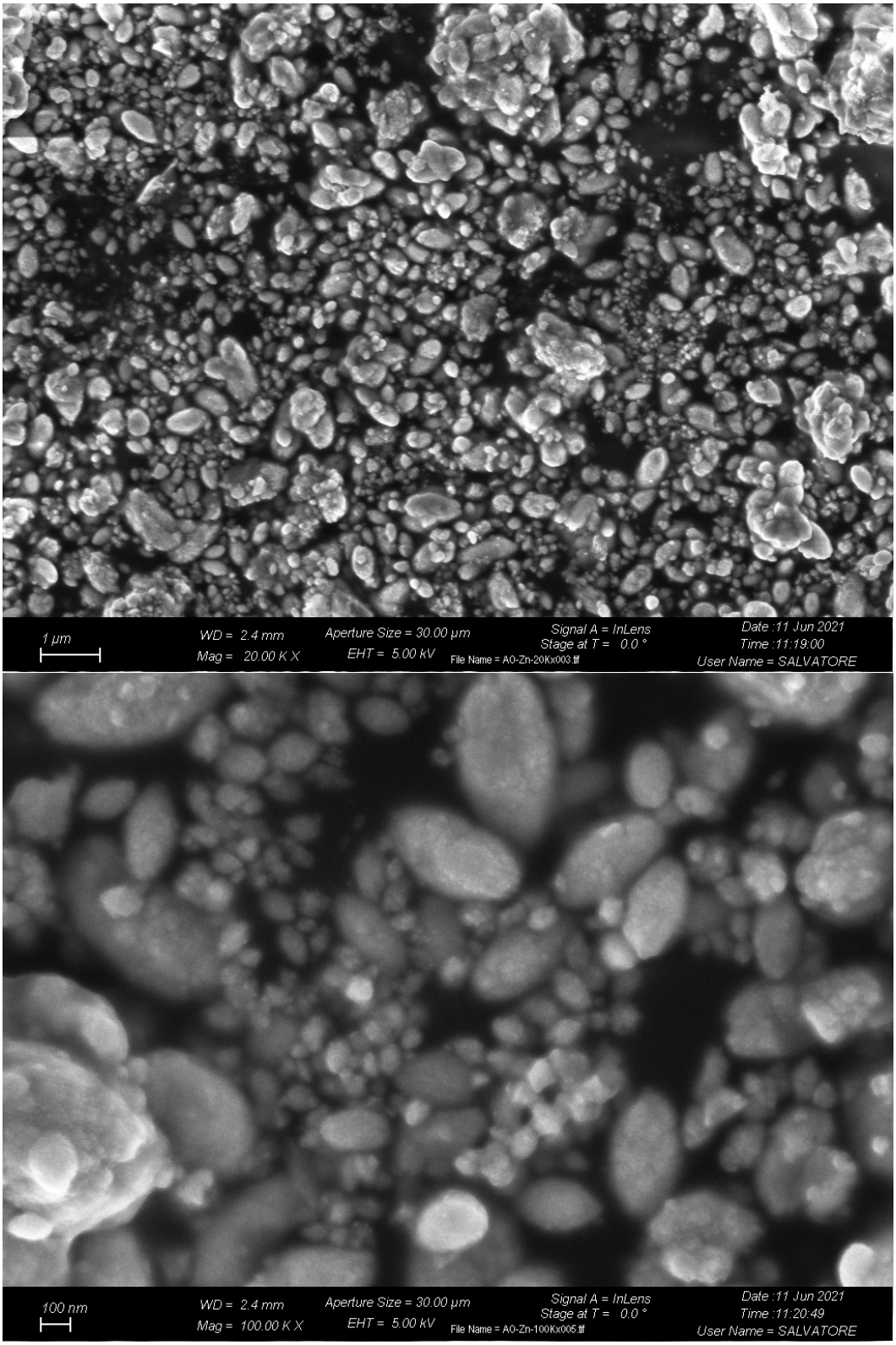

Figure 5.13: FESEM images of zinc ferrite nanoparticles

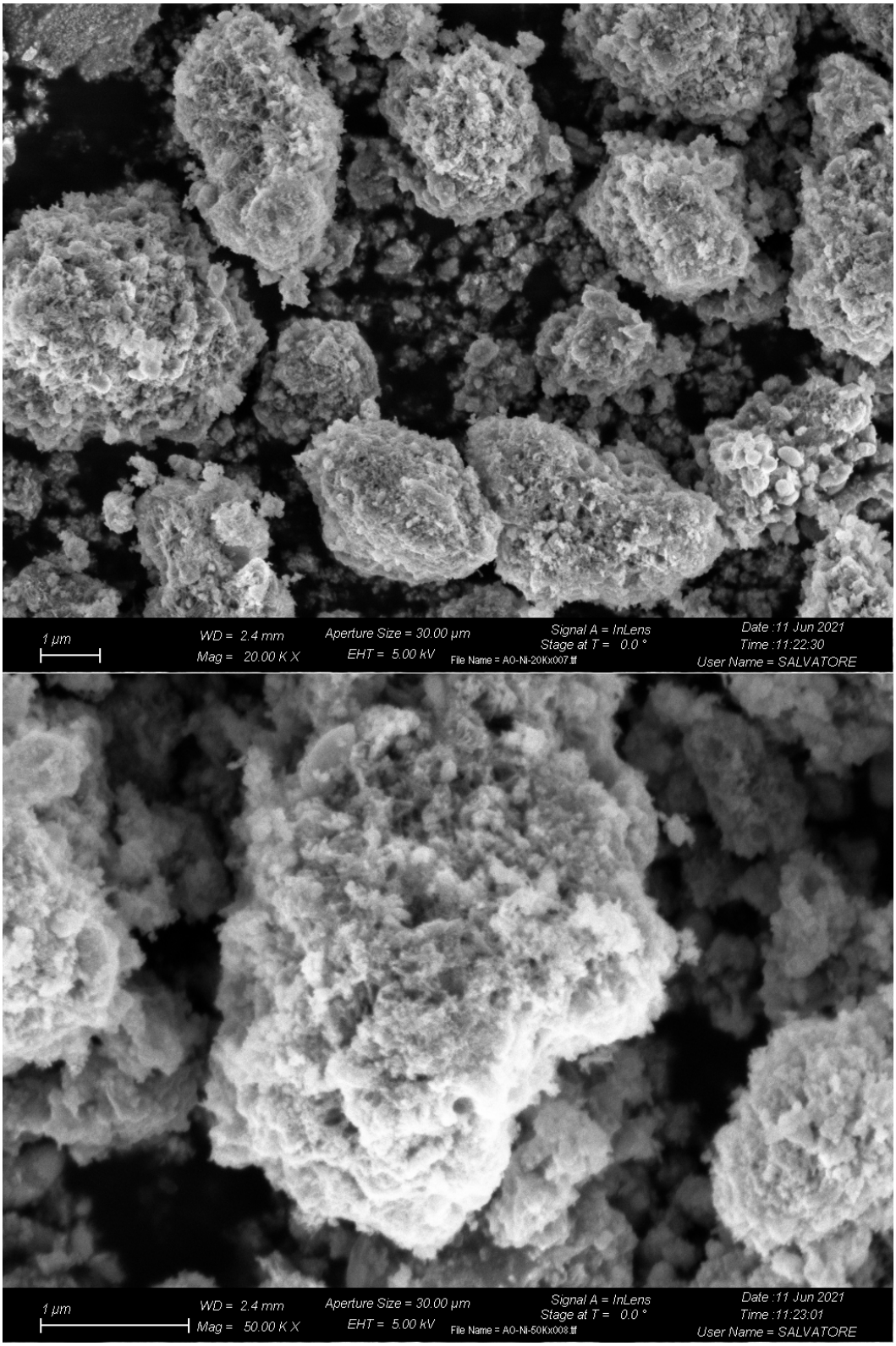

Figure 5.14: FESEM images of nickel ferrite nanoparticles

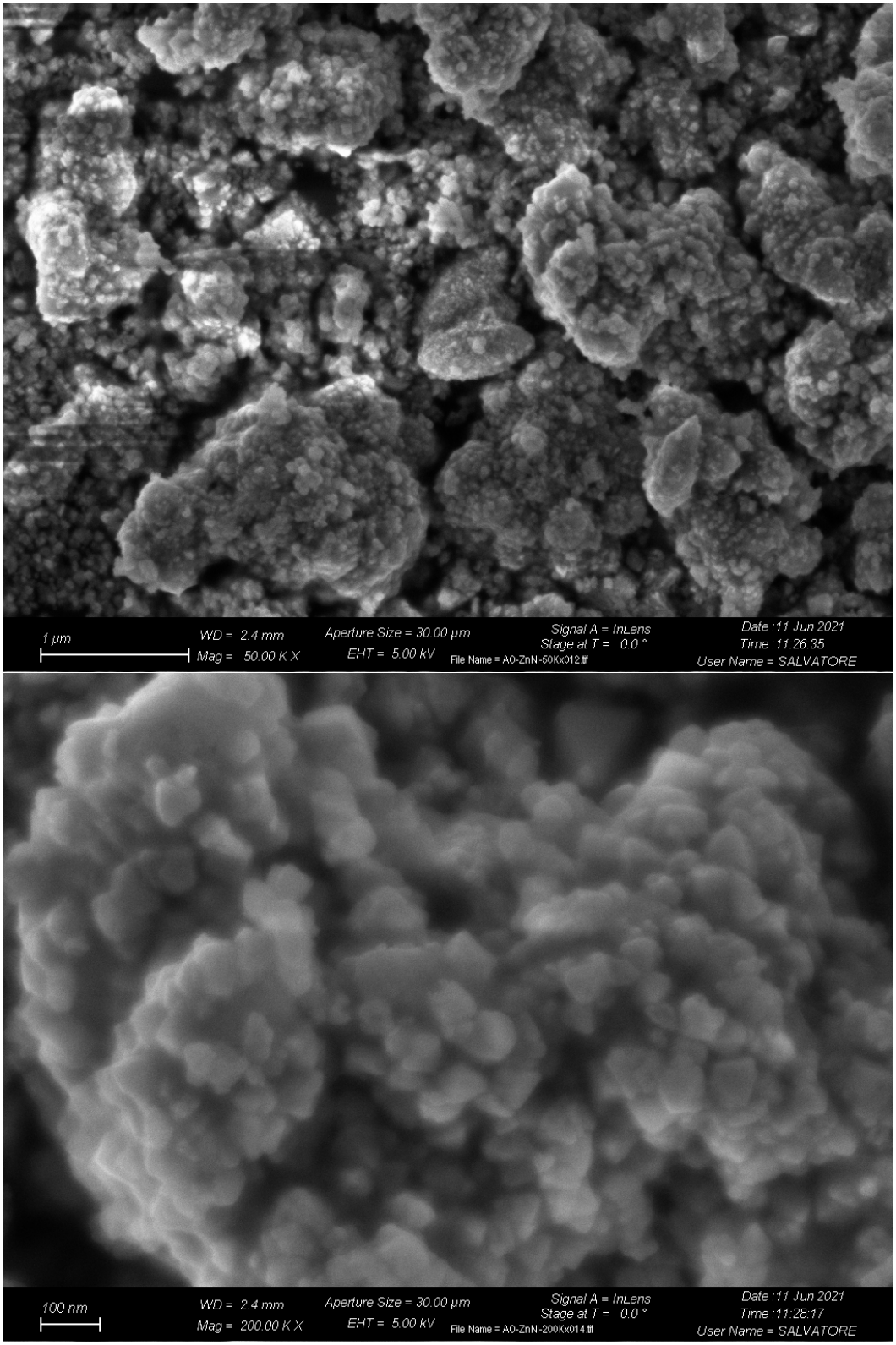

Figure 5.15: FESEM images of nickel-zinc ferrite nanoparticles

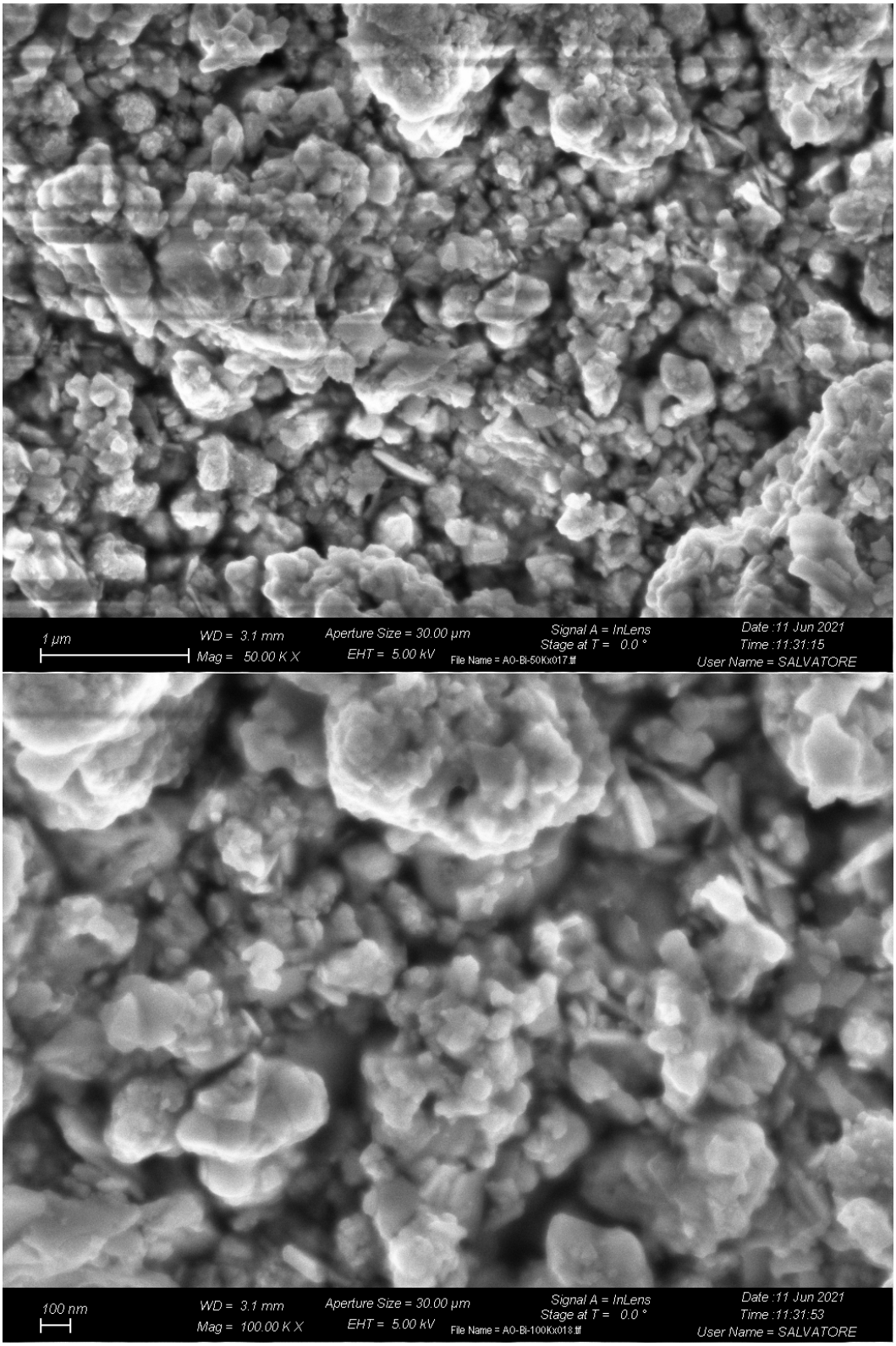

Figure 5.16: FESEM images of bismuth ferrite nanoparticles

Interestingly, the size distributions of the nanoparticles are quite sharp. Figure 5.17 shows the histograms relating to the size of the four ferrites with the average diameter of the FNPs. On the same graph the distribution function of the size is showed for each ferrite. Except for the ZNFO, which has a very close distribution to a Gaussian, the other approximating functions are lognormal distributions. Hence a more controlled and symmetrical size distribution was obtained for the nickel-zinc ferrite nanoparticles.

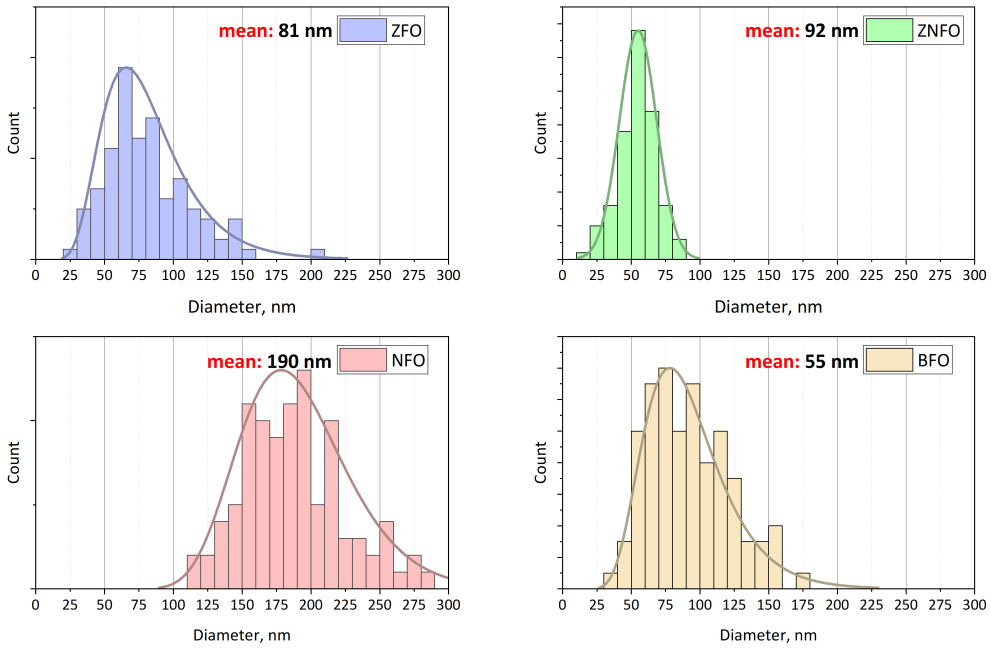

Figure 5.17: Particles size distribution histograms of prepared ferrite nanoparticles with the approximating distribution function

5.3.2 Raman

Raman analysis is among the best ways to characterize these nanoparticles. In fact, there are numerous sources in the literature on this type of analysis and it is relatively simple to compare the results obtained to understand the structure of the prepared ferrites. Figure 5.18 shows the obtained Raman spectra of the four FNPs. To better distinguish the peaks in order to increase the resolution, a red laser was used in the Raman optics ($\lambda = 785$ nm). Note that the drop at low Raman shifts is due to the notch filter of the Raman optics.

Finally, Tables 5.1, 5.2, 5.3 and 5.4 show the Raman modes observed by the analyzes of ZFO, NFO, ZNFO and BFO respectively and compare them

with the references found in the literature[70,71,72,73].

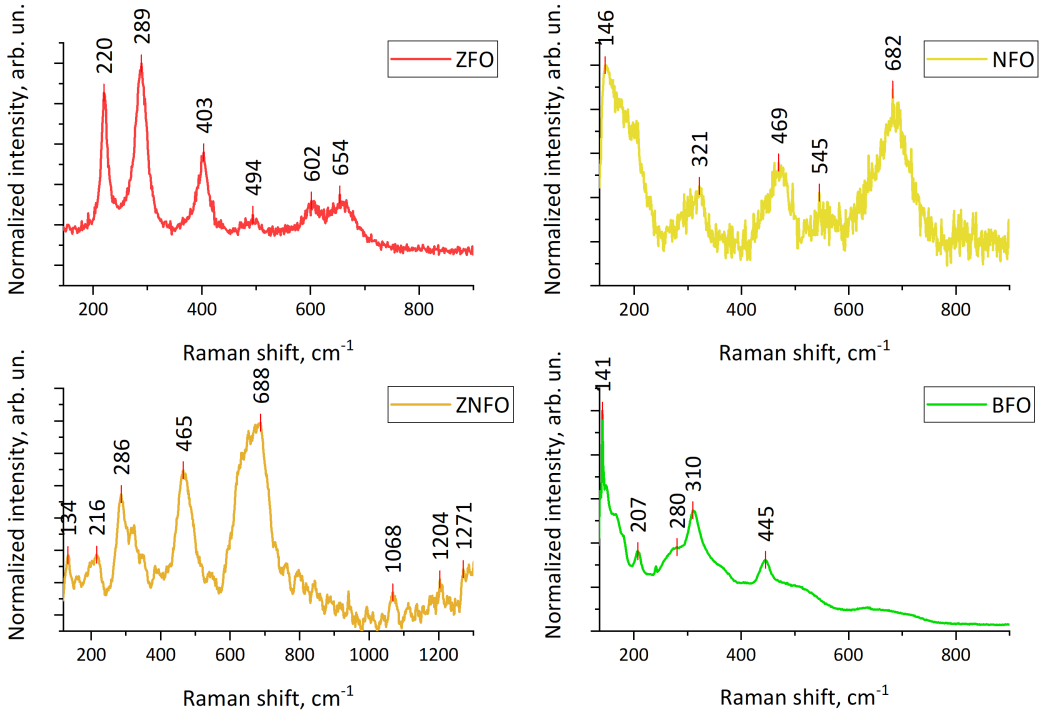

Figure 5.18: Raman spectra of prepared ferrite nanoparticles

[70]Rivero et al., "Synthesis and structural characterization of ZnxFe3-xO4 ferrite nanoparticles obtained by an electrochemical method".

[71]Kamble et al., "Domain size correlated magnetic properties and electrical impedance of size dependent nickel ferrite nanoparticles".

[72]Lazarević et al., "Nanodimensional spinel NiFe2O4 and ZnFe2O4 ferrites prepared by soft mechanochemical synthesis".

[73]Hashem and Hamed, "Preparation parameters optimization and structure investigation of multiferroic bismuth ferrite".

ZFO		
Mode	**Raman shift (reference)**	**Raman shift (this work)**
F_{2g} (1)	221 cm^{-1}	220 cm^{-1}
E_g	246 cm^{-1}	289 cm^{-1}
F_{2g} (2)	355 cm^{-1}	403 cm^{-1}
F_{2g} (3)	451 cm^{-1}	494 cm^{-1}
E_g	613 cm^{-1}	602 cm^{-1}
A_{1g}	647 cm^{-1}	654 cm^{-1}

Table 5.1: Raman modes of zinc ferrite and reference

NFO		
Mode	**Raman shift (reference)**	**Raman shift (this work)**
T_{2g} (1)	202 cm^{-1}	202 cm^{-1}
T_{2g} (3)	321 cm^{-1}	321 cm^{-1}
A_{1g}	468 cm^{-1}	469 cm^{-1}
T_{2g} (2)	555 cm^{-1}	545 cm^{-1}
A_{1g}	660-690 cm^{-1}	682 cm^{-1}

Table 5.2: Raman modes of nickel ferrite and reference

ZNFO		
Mode	**Raman shift (reference)**	**Raman shift (this work)**
F_{2g} (1)	213 cm^{-1}	216 cm^{-1}
T_{2g} (3)	333 cm^{-1}	322 cm^{-1}
A_{1g}	487 cm^{-1}	465 cm^{-1}
A_{1g}	705 cm^{-1}	688 cm^{-1}

Table 5.3: Raman modes of nickel-zinc ferrite and reference

BFO		
Mode	**Raman shift (reference)**	**Raman shift (this work)**
E_g	141 cm^{-1}	141 cm^{-1}
A_{1g}	210 cm^{-1}	207 cm^{-1}
E_g	277 cm^{-1}	280 cm^{-1}
E_g	301 cm^{-1}	310 cm^{-1}
E_g	433 cm^{-1}	445 cm^{-1}
A_{1g}	522 cm^{-1}	500 cm^{-1}

Table 5.4: Raman modes of bismuth ferrite and reference

5.3.3 FT-IR

Infrared spectroscopy is useful for analyzing the vibrational spectra of ferrites. In particular, from Figure 5.19 two peaks at 400-500 cm^{-1} can be seen for all four ferrites. These absorption peaks represent the vibrational levels of the crystal lattice of the Fe-O and X-O bond nanoparticles, respectively, where X = Zn, Ni and Bi. Given the relatively simple crystalline structure, FT-IR was used above all to test the purity of the samples obtained and to certify the complete evaporation of the solvent in the case of bismuth ferrite.

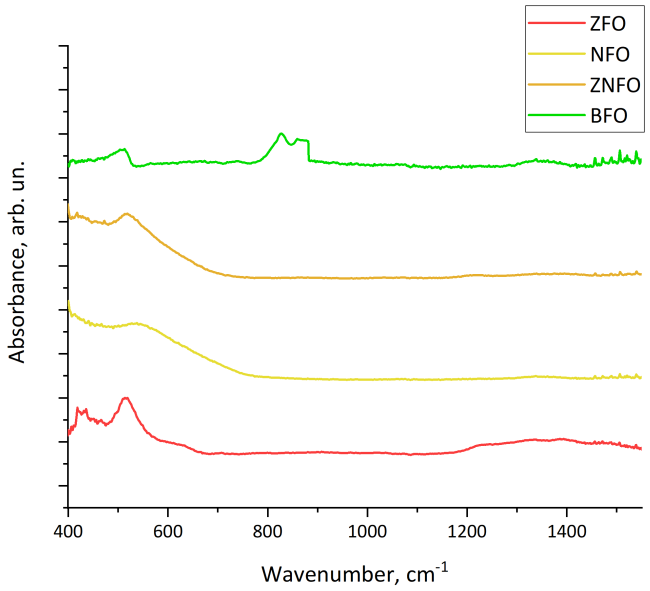

Figure 5.19: FT-IR spectra of ferrite nanoparticles

5.4 Ferrite-carbon dots conjugates

Numerous conjugation attempts have been made to find the one that is simpler, faster and with which a higher quality of interaction between the nanoparticles is obtained. As stated in section 4.4, an approach based on the dispersion of ferrites in an aqueous solution of CDs was chosen as the main protocol.

The conjugation is electrostatic, as it is due to an interaction between the π orbitals of the CDs, rich in aromatic rings and hybridized carbons, with the d orbitals of the metals of the ferrites (Figure 5.20). Another interaction mechanism could include coordination of the amino and hydroxyl groups with the ferrite orbitals.

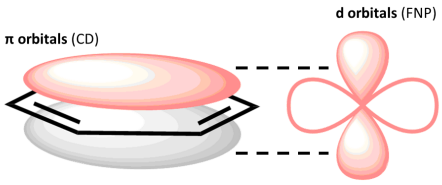

Figure 5.20: Conjugation mechanism between carbon dots and ferrites

5.4.1 FESEM

The electron microscope characterization of the Zn-CD, Ni-CD, ZnNi-CD and Bi-CD samples certified the successful conjugation between CDs and FNPs. Figures 5.21 and 5.22 show the FESEM images of the conjugations. As it can be seen, the CDs have created a homogeneous structure around the FNPs, albeit maintaining a morphology comparable to the initial one. It can also be noted that the CDs create a uniform structure that acts as an adhesive between the various ferrite nanoparticles. In aqueous solution the excess CDs will enter into solution and free the ferrite nanoparticles covered by an external shell of CDs that have interacted with them.

5.4.2 Raman

The Raman spectra of the CDs-FNPs conjugations are shown in Figure 5.23. As it can be seen, there is considerable evidence of the presence of both precursors in the spectra obtained. In particular, the peaks before 1000 cm^{-1} represent the modes of the ferrites discussed in the subsection 5.3.2, they are shifted due to the interaction between the electronic orbitals of the ferrites and the carbon dots. On the other hand, the peaks relative to the modes of the CDs

observed in the section 5.2.2 are still noted, in particular between 1100 and 2000 cm^{-1}. The disappearance of the band around 3000-3500 cm^{-1} is a further confirmation of the conjugation: the FNPs, interacting with the surface of the CDs, effectively inhibit the CH and OH ν modes of the functional groups.

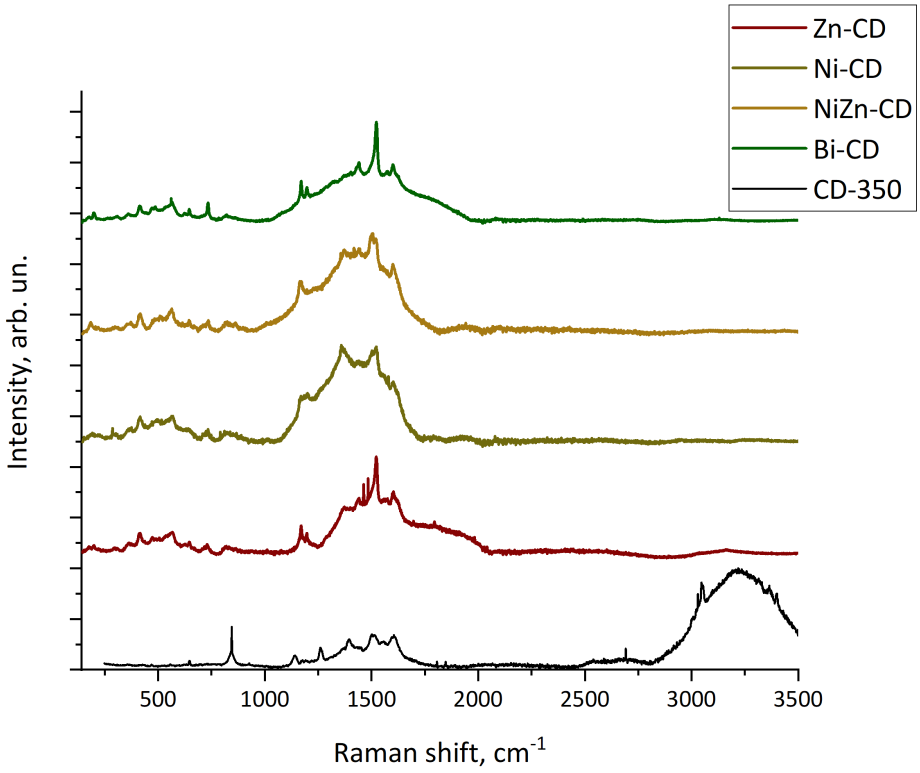

Figure 5.23: Raman spectra of conjugation products and the used carbon dots

5.4.3 FT-IR

A similar argument can be made for FT-IR analysis with respect to comments on Raman analysis. As it can be seen in Figure 5.24, in which the spectra, for each conjugation, of the CDs, of the ferrite and of the final product are compared, the vibrational modes of the ferrites in the final product of the conjugation are clearly present and recognizable. They are indicated by the purple circle. Furthermore, the vibrational modes related to the core and external shell of the CDs, already discussed in the section 5.2.1, are still visible.

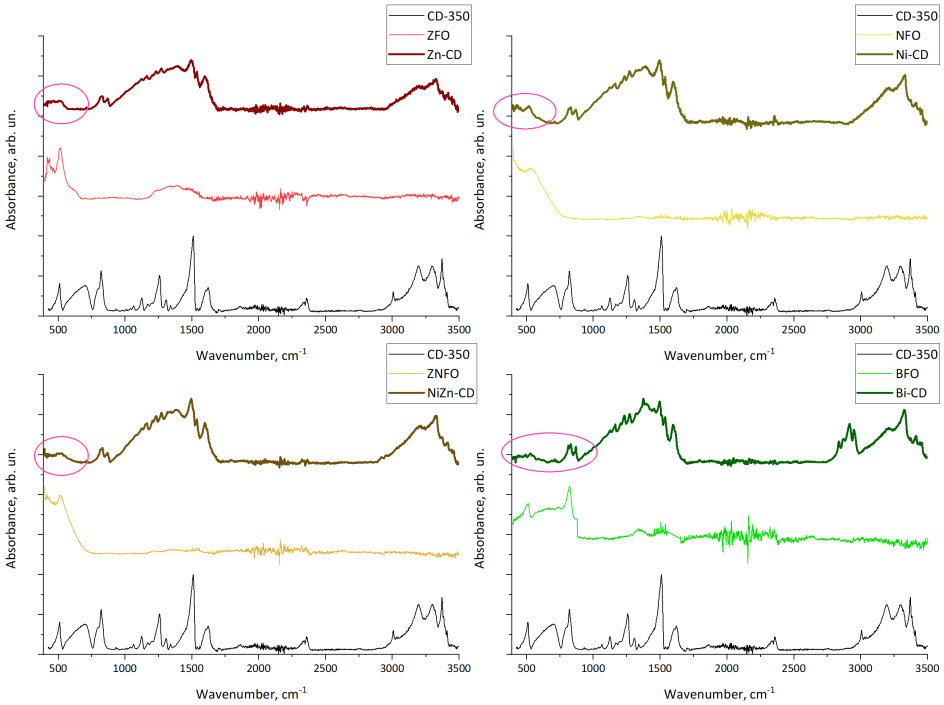

Figure 5.24: FT-IR spectra of conjugation precursors and products

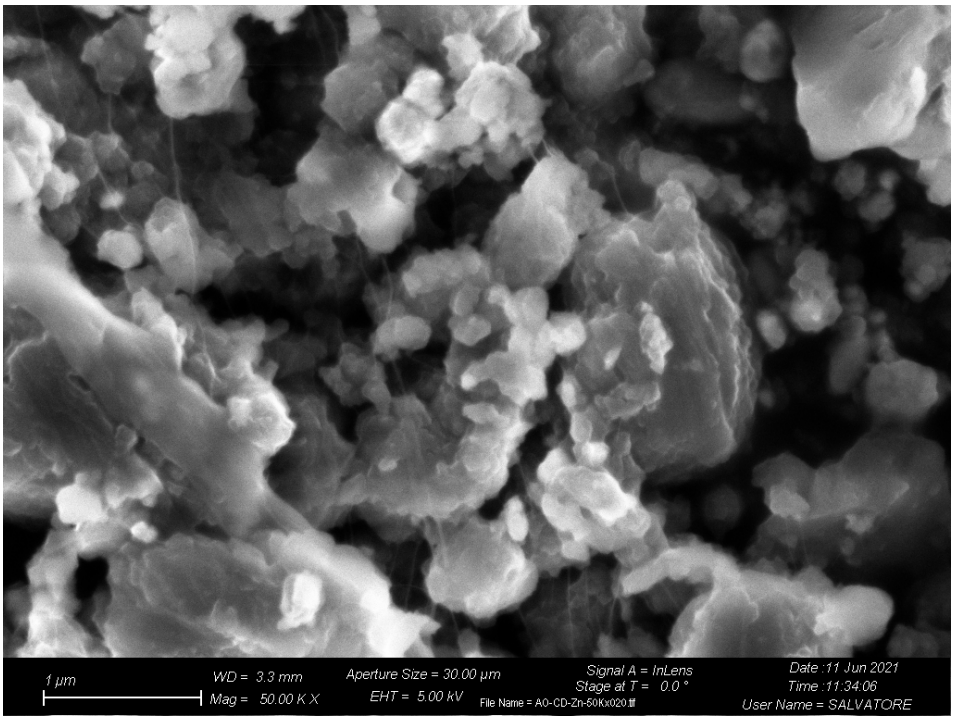

(a)

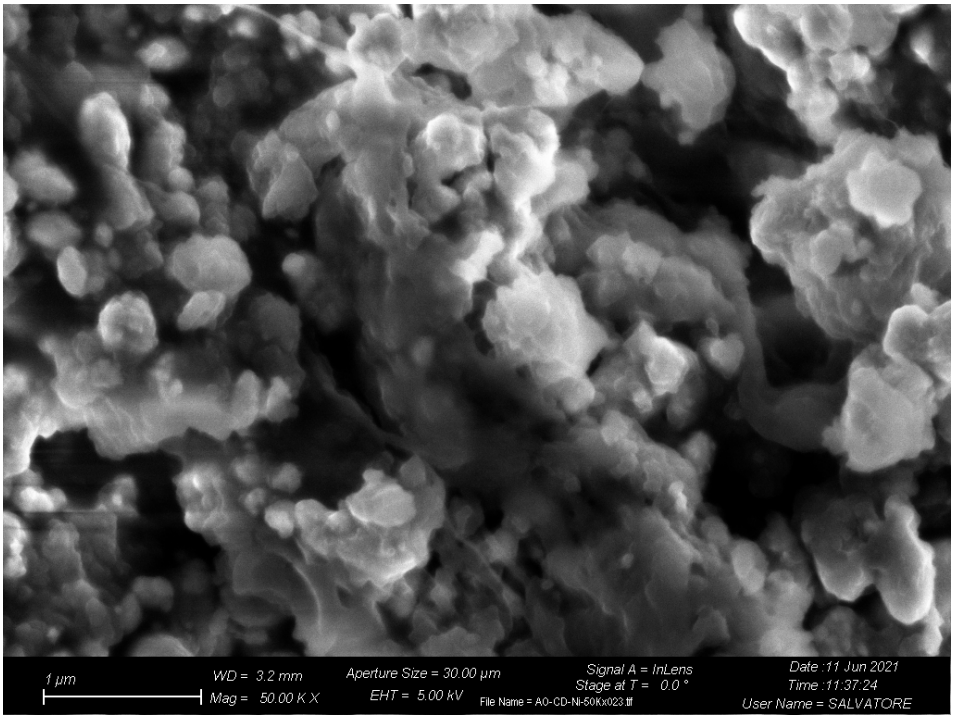

(b)

Figure 5.21: FESEM images of ferrite-conjugated carbon dots: a) Zn-CD and b) Ni-CD

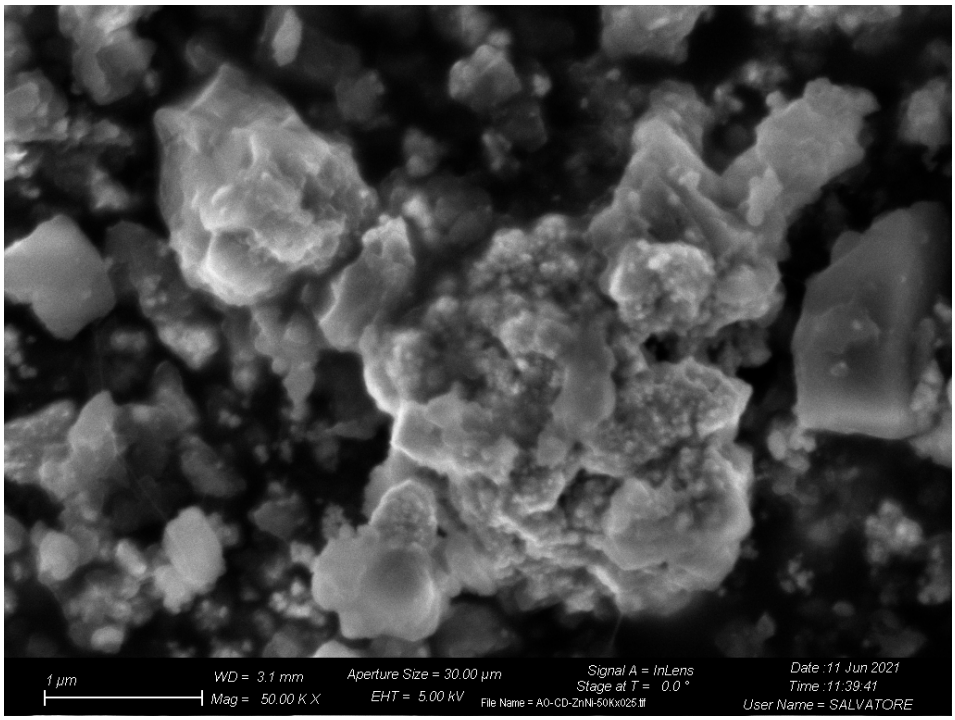

(a)

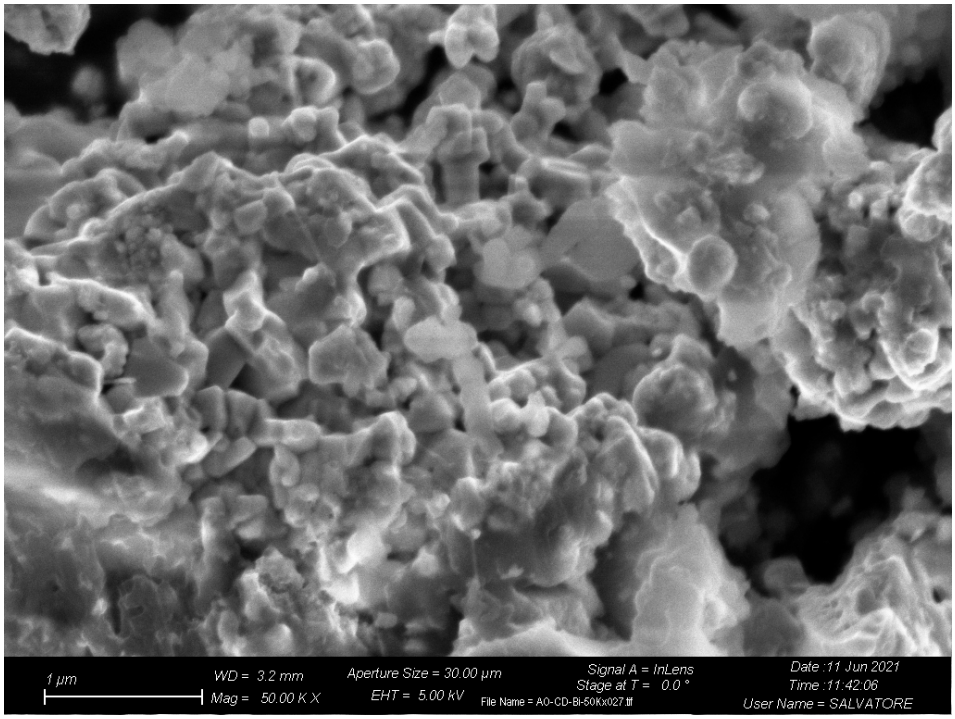

(b)

Figure 5.22: FESEM images of ferrite-conjugated carbon dots: a) ZnNi-CD and b) Bi-CD

Conclusions 6

This thesis project was carried out in the Carbon Lab of the Department of applied science and technology (DISAT) of the Politecnico di Torino between February and July 2021.

The work aims to synthesize and characterize CDs and FNPs of different metals (zinc, nickel and bismuth) and then proceed to their conjugation and subsequent characterization of the resulting samples. Both CDs and FNPs are compounds of particular importance in the biomedical field. In the thesis some characteristics of these nanoparticles are discussed and presented. CDs are extremely easy to synthesize, together with their biocompatibility and functionalizability. A peculiar property of these nanoparticles is in fact their surface which is rich in functional groups deriving from the precursors. They can be used as anchor sites for various biologically functional molecules or particles. The nanoparticles resulted to be highly water soluble. Furthermore, the carbon dots synthesized in this project exhibited interesting optical properties. In addition to an excitation-dependent photoluminescence, an excitation-independent photoluminescence emitting at 635 nm was detected, a radiation usable for imaging applications. Ferrite nanoparticles have properties linked to therapeutic uses. Their cytotoxicity, mainly linked to the presence of metal ions in the crystal lattice which can eventually create radical species and induce apoptosis, is reported by numerous papers. This property varies depending on the ferrite considered. The presence of iron III in nanoparticles suggests a possible application using the photo-Fenton effect in which an electron is transferred by the carbon dot to the ferrite after the absorption of a photon, creating Fe^{2+} ions capable of inducing oxidative stress. Another important characteristic of ferrites is their magnetism, a property that can be fundamental in drug delivery or hyperthermia processes. FESEM analysis of the prepared samples revealed spherical structures with diameters in the range of 50-100 nm, furthermore the samples showed good dispersibility in water. Finally, the CDs-ferrite conjugations were prepared following a simple conjugation protocol. The process showed good throughput and confirmation of conjugation occurred following Raman and FT-IR analyzes.

CDs were prepared following the procedure reported by Leblanc et al. in

their work 1. 0.56 g of p-phenylenediamine and 0.04 g of citric acid were mixed in 10 mL of DI water and then sonicated at 42 kHz for 1 hour. The resulting purple solution was put to dry in an oven at 80 °C for 48 hours. The precipitate was pounded in a mortar to be prepared for heat treatment. The next step consisted in processing the carbon dots samples under nitrogen gas in the muffle furnace. The next step will be treating the samples under argon gas in the muffle oven. Different temperatures made it possible to identify different sets of carbon dots. Four temperature values were used: 250 °C, 350 °C, 450 °C and 550 °C. The thermal process lasted for 10 minutes for all samples. Once extracted from the oven, the carbon dots were cooled to room temperature and subsequently dissolved in DI water for 10 minutes in a sonic bath to help dissolve and break up any aggregations. The obtained solution was then centrifuged at 10000 rpm for 10 minutes. After centrifugation, the residue was removed, and the liquid part dried at 80 °C for 48 h. In this way, only the carbon dots that were solubilized in water were obtained. Another set of carbon dots was prepared using polyethylene glycol as a non-ionic surfactant. In this case, a quantity of polyethylene glycol was added to the p-phenylenediamine and citric acid in a ratio of 1:1 with respect to citric acid. The heat treatment was done at 250 °C, and the centrifugation and extraction processes were the same as those of the other carbon dots.

For the preparation of the ZFO nanoparticles a solid-state reaction approach has been followed. Iron (III) nitrate and zinc nitrate quantities were taken to obtain a Fe:Zn molar ratio of 2:1. The salts were crushed in the mortar and subsequently treated at 550 °C for 1 hour under nitrogen gas in the muffle furnace. The preparation of the NFO nanoparticles followed a similar procedure. Iron (III) nitrate and nickel nitrate quantities were taken to obtain a Fe:Ni molar ratio of 2:1. After being pounded in the mortar they were treated at 550 °C in nitrogen gas for 1 hour. For ZNFO nanoparticles, a mole fraction of Fe:Zn:Ni equal to 2:1:1 was considered. Again, the salts were pounded in a mortar and then treated at 550 °C for 1 hour under nitrogen gas. The preparation of the BFO nanoparticles involved a sol-gel method. 5 mmol of Iron (III) nitrate and 5 mmol of bismuth nitrate were dissolved in 12 ml of ethylene glycol. To facilitate the dissolution, the compound was stirred at 80 °C for about 30 minutes. The obtained solution, brown in color, was placed in the muffle furnace under nitrogen gas preheated to 400 °C and with a temperature ramp of 5 °C/min. Once reached 650 °C the temperature was stabilized, and the compound calcined for 30 minutes. The resulting gray powder was then further calcined in air at 550 °C for 1h to remove any remaining solvent.

For the characterization part, the analyzes were carried out using Raman, FT-IR, fluorometer and FESEM equipment. The spectra and comments on the results are discussed in the thesis. In general, the analyzes carried out confirmed the hypotheses on the growth process and on the structure of both the carbon

dots and the prepared ferrite nanoparticles. The morphology appeared fairly homogeneous for almost all samples, with dimensions well within the nanoscale.

In conclusion, the results were satisfactory and lay a solid basis for future improvements, especially at the level of large scale manufacturing and characterization techniques, waiting for a future in which these technologies will finally be able to leave the laboratories to change millions of lives.

Acknowledgements 7

First of all, I would like to thank professor Alberto Tagliaferro for giving me the opportunity to work in this research group. These months have given me many interesting experiences that otherwise I would never have been able to live.

Thanks to dr. Mattia Bartoli, who followed me like a brother, infecting me every day with his passion and dedication. Thank you for letting me try, fail, and understand.

Thanks to Beppe and Paola because, needless to say, you have always believed in me, following my dreams. You are the best parents I could wish for. Thanks to Valeria, Salvatore, Alessandro and Leonardo, I love you.

Thanks to Martina. I could write a book of reasons, you already know everything. You have been my strength in many moments, I owe you a lot.

Thanks to Adele, Giacomo, Luca and Tommaso. This journey is just a parenthesis, but I am proud to have started it with you and I am sure it will continue like this for a long time.

Thanks to Maria for all the moments of intense joy and for the darkest ones, you have been an exceptional travel companion. Thank you for all the projects submitted at 11:59 PM, for sharing the anxiety of exams and sessions, and for infecting me with your kindness and simplicity.

Finally, thanks to all the people who have been close to me over the years. You've been an incredible boost, even just being happy for me for a passed exam.

Andrea Orlando

Bibliography

Alktranee, Mohammed. "Applications of nanotechnology with hybrid Photovoltaic/Thermal systems". In: *Journal of Applied Engineering Science* (Dec. 2020). ISSN: 1821-3197. DOI: 10.5937/jaes0-28760.

Nag, Anindya, Samta Sapra, and Subhas Chandra Mukhopadhyay. "Recent progress for nanotechnology-based flexible sensors for biomedical applications". In: *Handbook of Nanomaterials for Sensing Applications* (2021). DOI: 10.1016/B978-0-12-820783-3.00009-9.

Sangwan, Vinod K. and Mark C. Hersam. "Neuromorphic nanoelectronic materials". In: *Nature Nanotechnology* 15 (7 July 2020). ISSN: 1748-3387. DOI: 10.1038/s41565-020-0647-z.

Tang, Zhongmin et al. "Phosphorus Science-Oriented Design and Synthesis of Multifunctional Nanomaterials for Biomedical Applications". In: *Matter* 2 (2 Feb. 2020), pp. 297–322. ISSN: 2590-2385. DOI: 10.1016/J.MATT.2019.12.007.

Cheon, Jinwoo, Warren Chan, and Inge Zuhorn. "The Future of Nanotechnology: Cross-disciplined Progress to Improve Health and Medicine". In: *Accounts of Chemical Research* 52 (9 Sept. 2019). ISSN: 0001-4842. DOI: 10.1021/acs.accounts.9b00423.

Deng, Yudi et al. "Application of the Nano-Drug Delivery System in Treatment of Cardiovascular Diseases". In: *Frontiers in Bioengineering and Biotechnology* 7 (Jan. 2020). ISSN: 2296-4185. DOI: 10.3389/fbioe.2019.00489.

Kim, Jeonghwan, Antony Jozic, and Gaurav Sahay. "Naturally Derived Membrane Lipids Impact Nanoparticle-Based Messenger RNA Delivery". In: *Cellular and Molecular Bioengineering* 13 (5 Oct. 2020). ISSN: 1865-5025. DOI: 10.1007/s12195-020-00619-y.

Alafeef, Maha, Parikshit Moitra, and Dipanjan Pan. "Nano-enabled sensing approaches for pathogenic bacterial detection". In: *Biosensors and Bioelectronics* 165 (Oct. 2020). ISSN: 09565663. DOI: 10.1016/j.bios.2020.112276.

Nehra, Monika et al. "Nano-Biosensing Platforms for Detection of Cow's Milk Allergens: An Overview". In: *Sensors* 20 (1 Dec. 2019). ISSN: 1424-8220. DOI: 10.3390/s20010032.

Hu, Hailong. "Recent Advances of Bioresponsive Nano-Sized Contrast Agents for Ultra-High-Field Magnetic Resonance Imaging". In: *Frontiers in Chemistry* 8 (Mar. 2020). ISSN: 2296-2646. DOI: 10.3389/fchem.2020.00203.

Shin, Matthew D. et al. "COVID-19 vaccine development and a potential nanomaterial path forward". In: *Nature Nanotechnology* 15 (8 Aug. 2020). ISSN: 1748-3387. DOI: 10.1038/s41565-020-0737-y.

Dat, Nguyen Minh et al. "Synthesis, characterization, and antibacterial activity investigation of silver nanoparticle-decorated graphene oxide". In: *Materials Letters* 285 (Feb. 2021), p. 128993. ISSN: 18734979. DOI: 10.1016/j.matlet.2020.128993.

Zarei, Samira et al. "Theragnostic Magnetic Core-Shell Nanoparticle as Versatile Nanoplatform for Magnetic Resonance Imaging and Drug Delivery". In: *Biointerface Research in Applied Chemistry* 11 (5 Feb. 2021). ISSN: 2069-5837. DOI: 10.33263/BRIAC115.1327613289.

Ko, Wen Yin, Li Ting Huang, and Kuan Jiuh Lin. "Green technique solvent-free fabrication of silver nanoparticle–carbon nanotube flexible films for wearable sensors". In: *Sensors and Actuators, A: Physical* 317 (Jan. 2021), p. 112437. ISSN: 09244247. DOI: 10.1016/j.sna.2020.112437.

Li, Xin et al. "Antimicrobial nanoparticle coatings for medical implants: Design challenges and prospects". In: *Biointerphases* 15 (6 Nov. 2020). ISSN: 1934-8630. DOI: 10.1116/6.0000625.

al., Saeid Kargozar et. "Nanotechnology and Nanomedicine: Start small, think big". In: *Materials Today: Proceedings* 5 (7 2018). ISSN: 22147853. DOI: 10.1016/j.matpr.2018.04.155.

Choi, Young Hee and Hyo-Kyung Han. "Nanomedicines: current status and future perspectives in aspect of drug delivery and pharmacokinetics". In: *Journal of Pharmaceutical Investigation* 48 (1 Jan. 2018). ISSN: 2093-5552. DOI: 10.1007/s40005-017-0370-4.

Germain, Matthieu et al. "Delivering the power of nanomedicine to patients today". In: *Journal of Controlled Release* 326 (Oct. 2020), pp. 164–171. ISSN: 18734995. DOI: 10.1016/j.jconrel.2020.07.007.

Li, Tao et al. "Nanotechnology, an alternative with promising prospects and advantages for the treatment of cardiovascular diseases". In: *International Journal of Nanomedicine* Volume 13 (Nov. 2018). ISSN: 1178-2013. DOI: 10.2147/IJN.S179678.

He, Hongliang et al. "Survey of Clinical Translation of Cancer Nano medicines, Lessons Learned from Successes and Failures". In: *Accounts of Chemical Research* 52 (9 Sept. 2019). ISSN: 0001-4842. DOI: 10.1021/acs.accounts.9b00228.

Wong, Chi Heem, Kien Wei Siah, and Andrew W Lo. "Estimation of clinical trial success rates and related parameters". In: *Biostatistics* 20 (2 Apr. 2019). ISSN: 1465-4644. DOI: 10.1093/biostatistics/kxx069.

Bremer-Hoffmann, Susanne, Blanka Halamoda-Kenzaoui, and Sven Even Borgos. "Identification of regulatory needs for nanomedicines". In: *Journal of Interdisciplinary Nanomedicine* 3 (1 Apr. 2018). ISSN: 20583273. DOI: 10.1002/jin2.34.

Wu, Lin Ping, Danyang Wang, and Zibiao Li. "Grand challenges in nanomedicine". In: *Materials Science and Engineering C* 106 (Jan. 2020), p. 110302. ISSN: 18730191. DOI: 10.1016/j.msec.2019.110302.

Riggs, Jason E. et al. "Strong Luminescence of Solubilized Carbon Nanotubes". In: *Journal of the American Chemical Society* 122 (24 June 2000). ISSN: 0002-7863. DOI: 10.1021/ja9942282.

Mintz, Keenan J. et al. "A deep investigation into the structure of carbon dots". In: *Carbon* 173 (Mar. 2021), pp. 433–447. ISSN: 00086223. DOI: 10.1016/j.carbon.2020.11.017.

Peng, Zhili et al. "Carbon dots: promising biomaterials for bone-specific imaging and drug delivery". In: *Nanoscale* 9 (44 2017). ISSN: 2040-3364. DOI: 10.1039/C7NR05731H.

Pan, Dengyu et al. "Hydrothermal Route for Cutting Graphene Sheets into Blue-Luminescent Graphene Quantum Dots". In: *Advanced Materials* 22 (6 Feb. 2010). ISSN: 09359648. DOI: 10.1002/adma.200902825.

Dong, Yongqiang et al. "Blue luminescent graphene quantum dots and graphene oxide prepared by tuning the carbonization degree of citric acid". In: *Carbon* 50 (12 Oct. 2012), pp. 4738–4743. ISSN: 00086223. DOI: 10.1016/j.carbon.2012.06.002.

Tang, Libin et al. "Deep Ultraviolet Photoluminescence of Water-Soluble Self-Passivated Graphene Quantum Dots". In: *ACS Nano* 6 (6 June 2012). ISSN: 1936-0851. DOI: 10.1021/nn300760g.

Zhu, Shoujun et al. "Strongly green-photoluminescent graphene quantum dots for bioimaging applications". In: *Chemical Communications* 47 (24 2011). ISSN: 1359-7345. DOI: 10.1039/c1cc11122a.

Sheng, Yanshan et al. "pH-sensitive drug delivery based on chitosan wrapped graphene quantum dots with enhanced fluorescent stability". In: *Materials*

Science and Engineering C 112 (July 2020), p. 110888. ISSN: 18730191. DOI: 10.1016/j.msec.2020.110888.

Zheng, Xin Ting et al. "Glowing Graphene Quantum Dots and Carbon Dots: Properties, Syntheses, and Biological Applications". In: *Small* 11 (14 Apr. 2015). ISSN: 16136810. DOI: 10.1002/smll.201402648.

Xia, Chunlei et al. "Carbonized Polymer Dots with Tunable Room-Temperature Phosphorescence Lifetime and Wavelength". In: *ACS Applied Materials & Interfaces* 12 (34 Aug. 2020). ISSN: 1944-8244. DOI: 10.1021/acsami.0c11867.

Zhao, Qingnan et al. "Spectroscopic studies of the optical properties of carbon dots: recent advances and future prospects". In: *Materials Chemistry Frontiers* 4 (2 2020). ISSN: 2052-1537. DOI: 10.1039/C9QM00592G.

Liu, Meng Li et al. "Carbon dots: synthesis, formation mechanism, fluorescence origin and sensing applications". In: *Green Chemistry* 21 (3 2019). ISSN: 1463-9262. DOI: 10.1039/C8GC02736F.

Edison, Thomas Nesakumar Jebakumar Immanuel et al. "Microwave assisted green synthesis of fluorescent N-doped carbon dots: Cytotoxicity and bioimaging applications". In: *Journal of Photochemistry and Photobiology B: Biology* 161 (Aug. 2016). ISSN: 10111344. DOI: 10.1016/j.jphotobiol.2016.05.017.

Liu, JunJun et al. "One-Step Hydrothermal Synthesis of Nitrogen-Doped Conjugated Carbonized Polymer Dots with 31% Efficient Red Emission for In Vivo Imaging". In: *Small* 14 (15 Apr. 2018). ISSN: 16136810. DOI: 10.1002/smll.201703919.

Bao, Xin et al. "In vivo theranostics with near-infrared-emitting carbon dots—highly efficient photothermal therapy based on passive targeting after intravenous administration". In: *Light: Science & Applications* 7 (1 Dec. 2018). ISSN: 2047-7538. DOI: 10.1038/s41377-018-0090-1.

Zhou, Yiqun et al. "Nontoxic amphiphilic carbon dots as promising drug nanocarriers across the blood–brain barrier and inhibitors of β-amyloid". In: *Nanoscale* 11 (46 2019). ISSN: 2040-3364. DOI: 10.1039/C9NR08194A.

Liu, Mengli. "Optical Properties of Carbon Dots: A Review". In: *Nanoarchitectonics* 1 (1 Jan. 2020). ISSN: 2717-5332. DOI: 10.37256/nat.112020124.1-12.

Ma, Zhuoran et al. "Deep learning for in vivo near-infrared imaging". In: *Proceedings of the National Academy of Sciences* 118 (1 Jan. 2021). ISSN: 0027-8424. DOI: 10.1073/pnas.2021446118.

Jiang, Lei et al. “Photoactivated Fluorescence Enhancement in F,N-Doped Carbon Dots with Piezochromic Behavior”. In: *Angewandte Chemie International Edition* 59 (25 June 2020). ISSN: 1433-7851. DOI: 10.1002/anie.201913800.

Hu, Yaoping, Zhijin Gao, and Junfei Luo. “Fluorescence detection of malachite green in fish tissue using red emissive Se,N,Cl-doped carbon dots”. In: *Food Chemistry* 335 (Jan. 2021), p. 127677. ISSN: 18737072. DOI: 10.1016/j.foodchem.2020.127677.

Wang, Chun Chi et al. “Cu2+-induced quenching and recovery of the luminescence of dopamine-conjugated carbon dots for sensing deferasirox in plasma”. In: *Sensors and Actuators, B: Chemical* 311 (May 2020), p. 127916. ISSN: 09254005. DOI: 10.1016/j.snb.2020.127916.

Senapati, Kula Kamal, Chandan Borgohain, and Prodeep Phukan. “Synthesis of highly stable CoFe2O4 nanoparticles and their use as magnetically separable catalyst for Knoevenagel reaction in aqueous medium”. In: *Journal of Molecular Catalysis A: Chemical* 339 (1-2 Apr. 2011), pp. 24–31. ISSN: 13811169. DOI: 10.1016/j.molcata.2011.02.007.

Qu, Xiaolei, Pedro J.J. Alvarez, and Qilin Li. “Applications of nanotechnology in water and wastewater treatment”. In: *Water Research* 47 (12 Aug. 2013), pp. 3931–3946. ISSN: 18792448. DOI: 10.1016/j.watres.2012.09.058.

Lee, Hakho et al. “Recent Developments in Magnetic Diagnostic Systems”. In: *Chemical Reviews* 115 (19 Oct. 2015). ISSN: 0009-2665. DOI: 10.1021/cr500698d.

Reddy, L. Harivardhan et al. “Magnetic Nanoparticles: Design and Characterization, Toxicity and Biocompatibility, Pharmaceutical and Biomedical Applications”. In: *Chemical Reviews* 112 (11 Nov. 2012). ISSN: 0009-2665. DOI: 10.1021/cr300068p.

Maksoud, M. I.A. Abdel et al. “Synthesis and characterization of metals-substituted cobalt ferrite [Mx Co(1-x) Fe2O4; (M = Zn, Cu and Mn; x = 0 and 0.5)] nanoparticles as antimicrobial agents and sensors for Anagrelide determination in biological samples”. In: *Materials Science and Engineering C* 92 (Nov. 2018), pp. 644–656. ISSN: 09284931. DOI: 10.1016/j.msec.2018.07.007.

Larumbe, S. et al. “Sol-gel NiFe2O4 nanoparticles: Effect of the silica coating”. In: *Journal of Applied Physics* 111 (10 May 2012). ISSN: 0021-8979. DOI: 10.1063/1.4720079.

Thakur, Shweta, Radheshyam Rai, and Seema Sharma. “Structural characterization and magnetic study of NiFexO4 synthesized by co-precipitation

method". In: *Materials Letters* 139 (Jan. 2015), pp. 368–372. ISSN: 18734979. DOI: 10.1016/j.matlet.2014.10.014.

Zakiyah, Lall Beeharry et al. "Up-scalable synthesis of size-controlled copper ferrite nanocrystals by thermal treatment method". In: *Materials Science in Semiconductor Processing* 40 (Dec. 2015). ISSN: 13698001. DOI: 10.1016/j.mssp.2015.07.027.

Marinca, Traian Florin, Ionel Chicinaş, and Olivier Isnard. "Structural and magnetic properties of the copper ferrite obtained by reactive milling and heat treatment". In: *Ceramics International* 39 (4 May 2013), pp. 4179–4186. ISSN: 02728842. DOI: 10.1016/j.ceramint.2012.10.274.

Martínez-Rodríguez, Nelson Leonel, Sara Tavárez, and Zaira Isabel G. Sánchez. "In vitro toxicity assessment of zinc and nickel ferrite nanoparticles in human erythrocytes and peripheral blood mononuclear cell". In: *Toxicology in Vitro* 57 (June 2019). ISSN: 08872333. DOI: 10.1016/j.tiv.2019.02.011.

Al-Qubaisi, Mothanna et al. "Cytotoxicity of nickel zinc ferrite nanoparticles on cancer cells of epithelial origin". In: *International Journal of Nanomedicine* (July 2013). ISSN: 1178-2013. DOI: 10.2147/IJN.S42367.

Ahamed, Maqusood et al. "Oxidative stress mediated apoptosis induced by nickel ferrite nanoparticles in cultured A549 cells". In: *Toxicology* 283 (2-3 May 2011), pp. 101–108. ISSN: 0300483X. DOI: 10.1016/j.tox.2011.02.010.

Patade, Supriya R et al. "Preparation and characterisations of magnetic nanofluid of zinc ferrite for hyperthermia". In: *Nanomaterials and Energy* 9 (1 June 2020). ISSN: 2045-9831. DOI: 10.1680/jnaen.19.00006.

Egizbek, K. et al. "Stability and cytotoxicity study of NiFe2O4 nanocomposites synthesized by co-precipitation and subsequent thermal annealing". In: *Ceramics International* 46 (10 July 2020), pp. 16548–16555. ISSN: 02728842. DOI: 10.1016/j.ceramint.2020.03.222.

Staedler, Davide et al. "Cellular uptake and biocompatibility of bismuth ferrite harmonic advanced nanoparticles". In: *Nanomedicine: Nanotechnology, Biology, and Medicine* 11 (4 May 2015), pp. 815–824. ISSN: 15499642. DOI: 10.1016/j.nano.2014.12.018.

Rajaee, Azimeh et al. "Multifunctional Bismuth Ferrite Nanoparticles as Magnetic Localized Dose Enhancement in Radiotherapy and Imaging". In: *Journal of Biomedical Nanotechnology* 14 (6 June 2018). ISSN: 1550-7033. DOI: 10.1166/jbn.2018.2553.

Shahbazi, Mohammad-Ali et al. "The versatile biomedical applications of bismuth-based nanoparticles and composites: therapeutic, diagnostic, biosens-

ing, and regenerative properties". In: *Chemical Society Reviews* 49 (4 2020). ISSN: 0306-0012. DOI: 10.1039/C9CS00283A.

Rivero, María et al. "Synthesis and structural characterization of ZnxFe3-xO4 ferrite nanoparticles obtained by an electrochemical method". In: *RSC Advances* 6 (46 2016). ISSN: 2046-2069. DOI: 10.1039/C6RA04145K.

Kamble, Ramesh B. et al. "Domain size correlated magnetic properties and electrical impedance of size dependent nickel ferrite nanoparticles". In: *AIP Advances* 5 (1 Jan. 2015). ISSN: 2158-3226. DOI: 10.1063/1.4906101.

Lazarević, Z. Ž. et al. "Nanodimensional spinel NiFe2O4 and ZnFe2O4 ferrites prepared by soft mechanochemical synthesis". In: *Journal of Applied Physics* 113 (18 May 2013). ISSN: 0021-8979. DOI: 10.1063/1.4801962.

Hashem, H.M. and M.H. Hamed. "Preparation parameters optimization and structure investigation of multiferroic bismuth ferrite". In: *Materials Chemistry and Physics* 211 (June 2018). ISSN: 02540584. DOI: 10.1016/j.matchemphys.2018.03.012.